MINISTRY OF DEFENCE (PROCUREMENT EXECUTIVE)

AERONAUTICAL RESEARCH COUNCIL

CURRENT PAPERS

Decay of Trailing Vortices

By

E. H. Oon

Department of Aeronautical Engineering

University of Bristol

DECAY OF TRAILING VORTICES

by

E. H. Oon,
Department of Aeronautical Engineering,
University of Bristol

Communicated by Dr. J. W. Flower

SUMMARY

Models of elliptic, rectangular, swept and delta planforms were plunged vertically into a water tank and the vortex patterns on the surface were studied.

For each wing, the wake drift rate was found to increase with incidence and to decrease with increasing core separation.

The wake started off with discrete cores which grew independently and maintained their initial separation. The peak rotational velocity decayed as $\text{time}^{-\frac{1}{2}}$. The edges of the cores ultimately came very close together, and thereafter the wake descended as a system of interlocked cores which increased the separation between their centres with time. The velocity decayed as time^{-1}. There was a finite transition period between the two decay rates. This occurred at less than 10 s for the delta wing, about 20 s for the swept wing, about 30 s for the elliptic wing, and about 50 s for the rectangular wing.

The first phase of the wake development can be represented by a simple flow model of a single core of solid rotation surrounded by potential flow. The second phase was consistent with a flow model of a pair of cores, descending with constant linear momentum.

CONTENTS

CONTENTS

(continued)

SYMBOLS

a	eddy viscosity factor
a_0	two-dimensional lift-curve slope
a_1	three-dimensional lift-curve slope
b	wing span
b'	core separation
b_0'	initial core separation
c	velocity decay index
K	circulation of vortex
L	lift
r	radius of vortex
S	wing area
t	time
U	speed of model/aircraft
v	rotational velocity of vortex
v_t	peak rotational velocity
$\dot{z}$	wake drift rate
α	wing incidence
ϵ	eddy viscosity
ν	kinematic viscosity
ρ	air density
τ	constant value of $\dfrac{\nu t}{b_0'^2}$
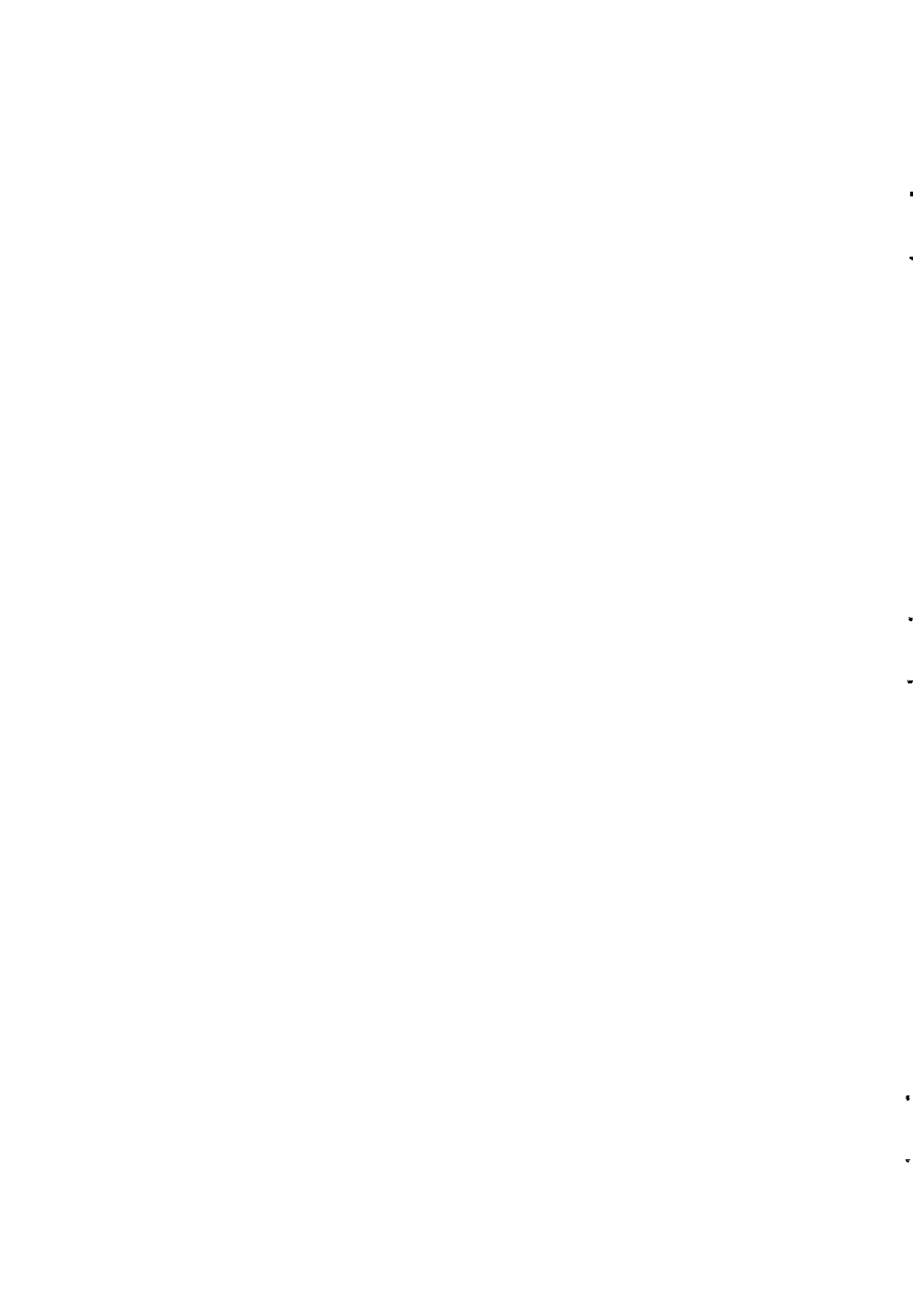
1. INTRODUCTION

Wing tip vortices generated in the wake of heavy aircraft are a hazard to following aircraft[1,2]. The problems are especially acute at take-off and landing, and steps taken to alleviate dangers to following traffic include time delays, landing long or taking off short[3]. But unnecessarily large aircraft separations in time or space reduce the efficiency of operations at busy airfields. Hence the need for detailed knowledge of the behaviour of vortex wakes.

Much experimental work involving flight measurements has been undertaken in the past. Two early experiments used, as wake-laying aircraft, a Meteor[4] and a Mustang[5].

In the Meteor test, the tracking aircraft flew alongside the wake, rendered visible by smoke, and traversed the vortices by edging in with its wing-tip pitot. In this way, measurements were made of the initial jet velocity and the inclination of the wake to the flight path. The rate of decay was investigated by the amount of aileron trim required to counteract the induced rolling moment which represented the most severe disturbance.

In the Mustang test, the probe aircraft penetrated the vortices transversely and recorded the disturbances with special instrumentation located at the nose. A more rapid rate of decay of the rotational velocity was observed after about 60 s. Up to 35 s, there was little change.

These early investigations drew upon classical aerodynamic theory, available in most textbooks (e.g. Millikan[6]), to compare with experimental results. Detailed work[7] had shown that two finite viscous cores were formed on completion of the rolling-up of the trailing vortex sheet. The rolling-up process is affected by the geometry of the wing, but a few spans downstream the classical horseshoe system is essentially correct.

Lamb's theory[8] on the effect of viscous forces on a single vortex was suggested as relevant though, at the time, no attempts were made to compare his work with the experimental results or to develop further theory taking into account the high Reynolds numbers in air.

Squire[9] suggested that the decay of a single trailing vortex depends on an eddy viscosity, ε, which is proportional to the circulation, K. The rotational velocity v at radius r and time t is:

$$v = \frac{K}{2\pi r}\left[1 - \exp\frac{-r^2}{4(\nu + aK)t}\right]$$

1.   (continued)

      where ν = kinematic viscosity

          a = eddy viscosity factor = ϵ/K.

In the typical conditions in air, ν is neglected compared with aK. From this, the maximum velocity v_t can be shown to decay as $t^{-\frac{1}{2}}$.

A series of tests were initiated at the Royal Aircraft Establishment to examine the validity of Squire's theory.

In the first experiment[10], a Devon probe aircraft used the aileron trim method behind a Lincoln wake-generating aircraft. Squire's theory with a = 0·0004 (as suggested by the Mustang[5] data) was applicable up to a wake age of about 150 s behind the Lincoln flying clean at 130 kt, after which rapid deterioration of the velocity was experienced.

The second test[11] involved transverse penetration of the wakes from a Comet and a Vulcan aircraft. Squire's theory held for the development of the velocity distribution through the vortices, although a value of a = 0·0002 gave better predictions. The downward drift of the wake was also found to agree with the theory in Ref. 3.

The formation of loops was observed for the first time far downstream of the Comet aircraft. Instability produced sinuous distortion of the vortex trails after about 40 s. The amplitude of the distortions increased with time till the trails joined up to form loops after about 90 s. Then rapid decay dissipated the loops in another 30 s or so.

Meanwhile, measurement of the wake behind a DC-8[12] flying at 25,000 ft indicated much less dissipation at high altitude.

The third investigation[13] used a Hunter aircraft for measurement of the wake motion near the ground. The wake drift results agreed with theory. The vortices spread apart as they descended, and crosswind components of wind could present a hazard by causing one vortex trail to remain along the runway. Loops formed by mutual interaction of a vortex trail with its image in the ground after less than 20 s.

From arguments assuming a constant shape of the developing wake, the time at which looping occurs was estimated, using the Comet and Hunter data, to be

$$t_{loop} \simeq \frac{10\rho U b^3}{L}$$

where ρ = air density,   U = speed of aircraft,

          b = wing span,   L = lift.

1. (continued)

This formula suggests loop formation for the Lincoln aircraft after about 125 s, which is the order of wake age when rapid decay was observed. In any case, the other tests have confirmed that, whether loops appear or not, the decay rate changes after a certain wake age is passed.

The fourth experiment[14], which was still in progress in August 1970, was undertaken to assess the difference in wake behaviour between a slender wing and conventional wings. The test is of practical significance for super-sonic transport aircraft.

The formation of the wake from a delta wing consists of a vortex sheet, springing from each leading edge and conically rolling up into a streamwise vortex before the flow passes the trailing edge. This contrasts sharply with the rolling up of the trailing vortex sheet from conventional wings.

The wake laid by a Handley-Page HP 115 research aircraft was penetrated transversely by a Morane-Saulnier MS 760 Paris aircraft fitted with special instrumentation.

For most of the wake age, the peak rotational velocity decayed as $time^{-1}$. It was suggested that the rapid decay could be associated with the phenomenon of vortex bursting for high incidences of a slender wing. This phenomenon was actually observed on the HP 115, when a sudden growth in core size was accompanied by disorganized flow in the core.

All the above experiments involved actual flight measurements. A common difficulty encountered was to ensure a traverse exactly through the centres. The smoke used to mark the vortices could be rapidly dispersed by atmospheric disturbances. In addition, the measurements themselves were subjected to the vagaries of atmospheric conditions, e.g. random turbulence, fluctuating wind velocities, etc.

Model studies can be more readily brought under control. However, there are practical problems which can detract from the attractiveness of control facilitation.

Due to the persistence of the wake from a conventional wing up to a long way downstream, a long wind tunnel would be necessary to observe the decay process in its entirety. For instance, even a moderate 50 lengths downstream would require a 25 ft working section for a 6-inch model.

Dragging models along a wire through a hangar, or through a towing tank, involves problems of instrumentation to measure the wakes at selected planes downstream of the model.

1. (continued)

The current report describes a simple technique of plunging models
vertically into a water tank and observing the vortex pattern on the surface.

1. (continued)

2. APPARATUS

Figure 1 shows the schematic layout of the apparatus. Details of the important items are shown in Figs. 2 - 7.

2.1 Water Tank

The cylindrical tank measured 7 ft deep and had a diameter of 5 ft. To gain access to it, the panel of the elevated floor over the top of the tank was removed. The tank was filled through a vertical pipe which opened near the bottom close to the wall of the tank.

2.2 Model Drive Mechanism

(See Figs. 2 - 4).

A box-like vertical rig carried the drive mechanism. The driving shaft was a hollow brass tube of ½-inch square cross section. It was connected through a system of step-down pulleys to a variable speed electric motor secured to the scaffolding of the elevated floor.

The pulley at the lower end of the rig was carried on a sprung shaft held down by a system of levers (Fig. 1). The shaft travelled along 2-inch slots in two end-plates (Fig. 3). When the trigger (Fig. 3) was hit by the pin connecting the driving shaft to the belt, the constraint on lever B (see Fig. 1) was removed and the pulley was carried up by the springs. The trigger then served to hold up the shaft.

The model wing was carried on a removable brass extension (Fig. 4). The triangular attachment was secured by a bolt and nut to the extension, the bolt being the centre of a small graduated scale.

2.3 Lighting and Photographic Equipment

A conventional double-reflex camera was mounted about 5 ft above the water surface so that a substantial portion of the surface appeared in the field of view (Fig. 6).

Two spotlights were positioned to shine across the tank onto mirrors (Fig. 5) which reflected the light over the water surface. The mountings of the spotlights and mirrors enabled them to be adjusted.

2.4 Measuring Devices

The microswitches were positioned 20·7 in apart and were connected to a chronometer (Fig. 7).

Two wooden rods of rectangular cross-section straddled the tank. Each had a similar rod of shorter length attached to its underside with flexible

rubber/...

2.4 (continued)

rubber strips over the remaining length at either end. The lower rod and
rubber strips skimmed the water surface of the full tank. One of these
composite rods carried a graduated scale on its upper surface (Figs. 4 and 6).

A clock was supported face up just above the water surface (Figs. 4 and 6).

2.5 Model Wings

The four model wings had the following planforms: elliptic, rectangular,
swept and delta. Their details are given in Table 1.

3. METHOD

3.1 Obtaining a Clean Surface

The location of the apparatus in the laboratory was such that oil spray was often present in the air around. Coupled with dust and dirt, this resulted in the formation of a sticky skin on the water surface after a day or so. A clean surface could be obtained by simply filling the tank up to overflow. But this measure invariably caused large-scale motion in the water which took a considerable time to be damped down.

A less time-consuming method was served by the two rods straddling the tank. By bringing them together and then drawing them apart, a clean surface was obtained without substantially disturbing the fluid below the surface.

In any case, the loss of water through evaporation entailed refilling the tank after about three days.

3.2 Starting and Stopping the Model

After it was switched on, the motor was allowed to reach its selected speed by holding the belt off the driver pulley. On releasing the belt, the model was started on its travel. The entry speed was deduced from the time taken to cover the distance between the microswitches.

When the pulley at the lower end of the rig was released, the tension was taken off the belt carrying the driving shaft. The trigger of the pulley release mechanism then held up the shaft and stopped the model near the bottom of the tank.

A tachometer detected variation in the model speed between entry and the end of its travel. By running the motor between about 1600 rpm and 2200 rpm, this variation was restricted to less than 15% of entry speed.

The wing incidence was measured with a clinometer.

3.3 Flow Visualization

By careful adjustment of the spotlights and mirrors, the desired uniform lighting over the surface was achieved.

The ideal flow visualization material should render visible not only the vortex cores but also the distribution of velocity through the vortices and the surrounding fluid. Lycopodium powder, paper punchings from data tape, sawdust and aluminium powder were tried in that order, before it was decided to use aluminium (see Fig. 8). When used sparingly, the lycopodium particles were too fine to reflect sufficient light with the lighting system employed. Too much of it obscured the velocity distribution through the wake. The

3.3 (continued)

sawdust was too coarse, and the paper punchings soaked easily and clumped together after a short time.

An interesting aspect of the tests was that with lycopodium, the boundaries of the wake system could be discerned fairly well. Fig. 8(b) shows an instance of looping at the surface observed during the tests

3.4 Photographic Record of Wake Patterns

The film used was 35 mm ASA 400. Depending on the magnitude of the rotational velocity, one of the following combinations of aperture and exposure was selected:

f 4, $\frac{1}{4}$ s ;   f 5·6, $\frac{1}{2}$ s ,   f 8, 1 s .

The exposure was changed in the middle of each sequence to follow the diminishing velocities.

The scale was arranged to appear down the edge of each frame (Fig. 6). The first frame was taken just as the model entered the water. Subsequent shots were discriminately taken according to changes in wake drift velocity and vortex structure. The time needed for resetting determined the limit to the interval between consecutive frames.

The idea of using a movie camera for measurements of rotational velocities was ruled out. The normal speed for shooting is about 20 frames a second, which means that each frame would only record the path travelled by a particle in about $\frac{1}{50}$ s, definitely not enough time to enable a reasonable streak to be seen on film.

4. RESULTS

Figures 9 - 14 show a selection of photographs depicting the behaviour of the wake. The time origin is taken to be the moment the model entered the water. Two sets of prints were used: (i) postcard size, with clock and scale included, for wake drift and core separation measurements, and (ii) enlargements, for measurement of the peak rotational velocity. Something like 300 prints were studied in all.

4.1 Wake Drift

In the case of two clearly formed vortices, the centre of the wake is the mid-point of the line joining their centres. Its position was read off the graduated scale. The datum was taken to be the path of travel of the trailing edge of the wing. The corresponding time was taken from the clock, which could be read to the nearest $\frac{1}{2}$ s.

Often, a number of secondary vortices appeared in addition to the main vortices (e.g. Figs. 9, 13 and 14). The interaction of two vortices of dissimilar strength and different or the same sense of rotation is described in Appendix A. By studying the flow pattern on the photographs, the directions of rotation of the secondary vortices were worked out. Some estimate was then made of the centre of such wake structure along the lines of the theory in Appendix A.

4.2 Core Separation

This is the distance between the centres of two distinctly formed vortices. Where secondary vortices appeared, the centre of each cluster of vortices was estimated. The distance between these centres then gave an approximate measure of the core separation.

4.3 Peak Rotational Velocity

Distinct streaks were sought out and their length measured. Where the streak had a large curvature, short lengths were stepped off. The velocity is the streak length divided by the exposure time.

The wake drift velocity was obtained from the tangent to the wake position vs. time graph. According to the position of the streak, an estimated correction was applied to the measured velocity to get the purely rotational velocity. Some check was afforded by choosing streaks at about the same radius, but at different positions around the core.

Figures 15 - 18 indicate the behaviour of the vortex wakes from the four model wings. Each graph treats the variations of wake drift, core separation and peak rotational velocity with time.

4.4/...

4. (continued)

4.4 Non-Dimensionalized Velocity Decay

It is desirable to have the variables appropriately non-dimensionalized to encompass the effects of scale, wing geometry, incidence, model speed, viscosity of the fluid, etc.

The initial core diameter on completion of the rolling-up of the trailing vortex sheet from an elliptic wing is proportional to the initial core separation, b_o' [7]. This together with Squire's theory, suggests a non-dimensional velocity to be

$$\frac{v_t \, b_o'}{K} \quad ,$$

where K = circulation of vortex,
and a non-dimensional time to be

$$\frac{vt}{b_o'^2} \quad .$$

There are two ways of obtaining the value of K in the experiment.

(i) K can be deduced from the wing characteristics, incidence and model speed by using the relation

$$K = \frac{L}{\rho U b_o'} = \frac{a_1 \alpha U S}{2 b_o'}$$

where a_1 is the three-dimensional lift curve slope. Thus, another non-dimensional velocity could be

$$\frac{v_t b_o'^2}{a_1 \alpha U S}$$

The value of a_1 was obtained from the Royal Aeronautical Society data sheets[15]. The tests were carried out at a Reynolds number of about 2×10^4, from which a_o was estimated to be about 4·4 per radian. A check was made using the formula from Abbott and von Doenhoff[16] (see Table 1).

The zero-lift incidence for the rectangular wing was estimated to be about -3° by invoking the analogy of a symmetrical section with 50% chord deflected 7° downward.

For the delta wing, previous measurements with similar sections[17] have shown the zero-lift incidence to be less than 1°. No correction was applied to the measured incidence.

Since the tests have all been conducted in water, the non-

4.4 (i)   (continued)

dimensional time could be represented by

$$\frac{t}{b_o'^2}$$

Fig. 20 shows a plot of $\frac{v_t b_o'^2}{a_1 \alpha US}$ vs. $\frac{t}{b_o'^2}$. The upper bounds

from the HP 115 tests[14] are included after reduction to these variables.

(ii) K can also be estimated from the wake drift velocity

$$\dot{z} = \frac{K}{2\pi b'} \quad .$$

This velocity was obtained from the gradient to the wake drift curve at the point near the origin corresponding to the measured b' value.

Using this K, Fig. 21 was plotted of $\frac{v_t b_o'}{K}$ vs. $\frac{t}{b_o'^2}$. The

HP 115 upper bounds are included.

5. DISCUSSION

5.1 Arbitrary Time Origin

The rolling up of the trailing vortex sheet behind a conventional wing takes a small but finite time to be completed. The age of the vortex wake has often been reckoned from the time when the two discrete cores are formed. The time origin adopted in the experiment (see Section 4) therefore results in some error if the measured time is to represent wake age defined as above. However, the error would materially affect only the early wake ages. In any case, it is difficult to make any precise correction since the wake drift origin was also arbitrarily defined (Section 4.1). For the slender wing, the error is in the opposite direction, since the leading edge vortex sheets roll up before the sheet passes the trailing edge.

In the theory in Appendices C and D, the origin of wake age is taken to be the limit as the peak rotational velocity tends to infinity. In practice, this would mean a point of time before the cores were formed. Again, taking the measured time as wake age would result in substantial errors only for early wake ages.

5.2 Effect of Wall of Tank

Appendix B analyses the interaction of the vortices with their images in the wall of the tank.

The vortices started off at about 10 in from the edge of the tank, their initial separation distance being something of the order of 6 in. This initial disposition should lead to a maximum error of about 12% of the true wake drift velocity (the measured velocity is less than the true value). Theoretically, the vortices should also be impelled towards each other with a speed which is about 3% of the drift velocity.

For the elliptic, swept and delta wings, these errors were not seriously considered since the vortices were relatively close together to begin with. However, in the case of the rectangular wing, it is likely that these errors have contributed to the flattening of the wake drift curve near the origin (Fig. 16(a)).

5.3 Effect of Model Speed Variation during Travel

Additional vortices will be continually shed off an accelerating wing. Since the circulation, K, is proportional to the model speed, there would have been a maximum change of 15% in K between entry and the stopping of the model (see Section 3.2). However, this change was spread over a distance of

5.3 (continued)

about 7 ft and would not be expected to alter substantially the vortex pattern at the surface.

5.4 Path Lines and Streamlines

The flow pattern captured on film does not reveal the streamlines since the picture is not one of steady flow. It only shows the path travelled by a particle over the period of time that each frame was exposed.

By plotting both the streamlines and path lines using the appropriate functions for a vortex pair (readily available in most textbooks, e.g. Ref. 18, or easily derived), it was found that the distance between apparent centres is greater than that between real centres by about 10% of the latter. (See Fig. 22 for an illustration of the velocity distribution through the wake from the delta wing).

This correction was not applied to the core separation measurements. At early wake ages, the effect of the wall of the tank was to draw the vortices together (Section 5.3). In any case, for wakes where secondary vortices appeared, the errors likely to be incurred in estimating the core centre would make such a correction meaningless.

5.5 Discussion of Flow Patterns in Figs. 9 - 14

To avoid repetition later, some comments are now made on the flow patterns shown on the photographs in Figs. 9 - 14.

Fig. 9 Elliptic wing, $\alpha = 12^{\circ}$, U = 2·0 ft/s

At the same time as the cores grew, they moved apart. After 18 s, there appeared some slight distortion of the port vortex. After 35 s, a cluster of at least three vortices had replaced the port vortex, while the starboard vortex had at least two secondary vortices above it. From then on the pattern became increasingly distorted, but the maximum velocity remained around the centre of the wake. The distance between the two clusters of vortices progressively narrowed.

Fig. 10 Rectangular wing, $\alpha = 5^{\circ}$, U = 3·0 ft/s

A contra-rotating secondary vortex appeared around the port vortex after 27 s. This was most probably caused by the fluid coming from behind the driving shaft. It was soon absorbed into the main vortex.

The cores maintained their initial separation even after 40 s. Their discrete nature is evident. The rolling up of the streaks of fluid devoid of aluminium particles shows to good advantage the entrainment of the surrounding

fluid/...

5.5 (continued)

<u>Fig. 10</u> (continued)

fluid in the growth process of the cores. At 72 s, the maximum velocity
appeared to be near the centre of the wake. After 130 s, the cores, full-
grown, could just be made out, with the fluid still moving fastest around the
wake centre.

<u>Fig. 11</u>   Rectangular wing, $\alpha = 10^{\circ}$,   U = 2·2 ft/s

The discrete nature of the vortices is clear for the early wake ages.
Between 35 and 70 s, fluid seemed to be moving across the lower boundary of
the wake system. But the streaks are path lines, not streamlines. Apart from
changes in the magnitude of the velocities, the patterns from 70 s onwards
appeared to be similar, with the maximum velocity around the wake centre.

<u>Fig. 12</u>   Swept wing, $\alpha = 12^{\circ}$,   U = 2·0 ft/s

At 4·5 s, the cores appeared separate, but at 18·5 s, they seemed to have
grown to touch each other. There was some reduction in their separation
distance during the interval. After about 20 s, the maximum velocity
persisted around the wake centre as the cores drew apart.

The port vortex was slightly distorted after 35 s. At least two second-
ary vortices could be discerned above it at 47 s.

<u>Fig. 13</u>   Delta wing, $\alpha = 5^{\circ}$,   U = 2·6 ft/s

An undistorted pattern of an interlocked pair of cores persisted up to
20 s, at which a slight distortion of the port vortex appeared. By 27 s, two
clusters of secondary vortices characterized the wake pattern. Throughout,
the maximum velocity remained around the wake centre.

<u>Fig. 14</u>   Delta wing, $\alpha = 12^{\circ}$,   U = 2·4 ft/s

After 1C s, a void appeared suddenly between and slightly above the
vortices which were thrust apart. Some fluid appeared to be thrown up from
below. The observation conforms with the presence of a vortex with its plane
of rotation normal to the surface, and suggested looping just beneath the
surface.

The cores came together again from 15 s to 25 s. A secondary vortex
spiralled its way into the port vortex during this period. From the flow
pattern between them, it was deduced that they rotated in the same sense. The
two vortices seemed to swing each other round in a clockwise sense, which
agreed with the theory in Appendix A.

5.5 (continued)

The features of the wake patterns described above are typical, and one or more of them appeared at various occasions during the other tests.

5.6 Wake Drift and Core Separation

(See Figs. 15 - 18).

Generally, the wake drift rate was found to increase with incidence (none of the wings was stalled) and to decrease with increasing core separation. This is in agreement with theory. No definite conclusions can be drawn concerning the effect of model speed, since the speed range used was small, but the results for the rectangular wing show an increase in the drift rate with speed.

The vortices shed from the rectangular wing retained their original separation for quite a long time. Some sinuous distortion appeared after about 30 s which progressively increased. Looping at the plane of the surface was observed on one of the tests ($\alpha = 10^\circ$, U = 2·6 ft/s) at about 100 s. It is reasonable to suppose that this is the order of wake age when looping could have occurred for the other tests, though, of course, not all looping would happen to be at the surface. It was around this time, too, that clusters of secondary vortices appeared for one of the other tests ($\alpha = 10^\circ$, U = 3·1 ft/s). In all cases, the beginning of substantial change in the original core separation was associated with the onset at about 60 s of a wake pattern where the maximum rotational velocity was around the wake centre. When the cores appeared discrete, they always maintained their initial separation.

This interesting observation was pursued further with the other wings.

For all tests on the delta wing, the wake pattern of maximum velocity around the centre was observed almost right from the start. The core separations increased markedly after about 5 s. Secondary vortices appeared for all the tests: at 25-40 s for $\alpha = 5^\circ$, 15-25 s for $\alpha = 8^\circ$, and about 10 s for the higher incidences. The "looping beneath surface" phenomenon on one test ($\alpha = 12^\circ$, U = 2·4 ft/s) has been mentioned (see Section 5.5).

For the swept wing and the elliptic wing, the change in wake pattern began after about 25 s. Again the core separations at this wake age were beginning to show appreciable increases from their initial values. Secondary vortices appeared at 30-45 s.

There is strong evidence, therefore, that the development of the wake can be broadly divided into two regions. Initially, the vortices are formed

as discrete/...

5.6 (continued)

as discrete cores which behave independently of each other. As the cores
grow, due to the action of viscous forces, their edges ultimately come
extremely close together. After this point has been reached, the cores no
longer remain independent of each other. They intermix and the whole system
of two locked cores grows with wake age, appearing to maintair the same shape
until their mutual interference leads to the formation of clusters of
secondary vortices.

The similarity in behaviour among all the wings suggests the existence
of some non-dimensional parameters which may make the experimental data
collapse into a single curve.

5.7 Velocity Decay

A difficulty experienced in measuring the rotational velocity at very
early wake ages was that an exposure too long produced streaks merging into
one another, so that it was hard to tell where one streak ended and the next
began. In such cases, there is the likelihood that the distinct streaks
selected may not represent the maximum velocity.

The graphs of peak rotational velocity vs. time in Figs. 15 - 18 confirm
that there are two different decay rates. Lines of slope $-\frac{1}{2}$ and -1 fitted
the data at early and late wake ages respectively. There appears to be a
finite transition period between the slow and the rapid decay rates, and this
is clearly evident from the results of the elliptic wing and the rectangular
wing.

The beginning of the transition period was at about·

$$30 \text{ s for the elliptic wing}$$

$$50 \text{ s }^{"} \quad ^{"} \text{ rectangular wing}$$

$$20 \text{ s }^{"} \quad ^{"} \text{ swept wing}$$

$$10 \text{ s }^{"} \quad ^{"} \text{ delta wing}$$

These are of the same order as the wake ages when change in the wake shape
was observed, which were:

$$25 \text{ s for the elliptic wing}$$

$$60 \text{ s }^{"} \quad ^{"} \text{ rectangular wing}$$

$$25 \text{ s }^{"} \quad ^{"} \text{ swept wing}$$

$$<5 \text{ s }^{"} \quad ^{"} \text{ delta wing}$$

The conclusion is reached that the transition to a more rapid decay rate is
associated with the change in wake pattern observed for the variation of core
separation.

5.7 (continued)

The decay rate lines drawn in Figs. 15 - 18 are reproduced on a single graph in Fig.19. This graph strongly suggests that while a supersonic transport aircraft may have a much higher rotational velocity initially in its wake than a conventional heavy transport, due to its shorter span, the rapid decay rate over almost all its wake age is likely to cause the wake to be dissipated much faster than that of the conventional aircraft.

In Fig. 20 the data appear to collapse into a single curve, although there is some scatter. A greater degree of scatter is seen in Fig. 21, mainly attributable to the errors incurred in deducing K from the wake drift velocity. The abscissae in these figures is, for the model results, proportional to the non-dimensional time suggested in Section 4.4, where only the kinematic viscosity (a constant for these tests) has been omitted. The upper bounds of the results from the HP 115 tests, with time scaled by the ratio of the eddy viscosity of air to the kinematic viscosity of water, are shown for comparison. The proximity of these bounds, carried out with a 'model' of very large scale, at a much higher Reynolds number, in a different fluid, seems to justify the parameters used.

It can be postulated that, in theory, the peak rotational velocity decays according to a single law expressed as

$$\frac{v_t b_o'}{K} \quad \alpha \quad \left\{ \frac{\nu t}{b_o'^2} \right\}^{-c}$$

where the index $c = \frac{1}{2}$ for $\dfrac{\nu t}{b_o'^2} < \tau$,

$= 1$ for $\dfrac{\nu t}{b_o'^2} > \tau$,

where τ is some constant.

From the graphs, τ was estimated to be between 3×10^{-3} and 6×10^{-3}.

Some reservation must be made about the applicability of this law to the wake in the vicinity of the aircraft, because of the different nature of formation of the vortices from a slender wing and from conventional wings.

All the vortices must start off as discrete cores, but their growth ultimately brings them very near each other. How soon this will be depends very much on the wing characteristics and the scale. Fig. 22 illustrates the different wake structures between the wake from the delta wing and that from the rectangular wing, nearly four times as old.

Corresponding to the two decay rates, two basic vortex models can be advanced to represent the development of the wake, viz. (i) a single vortex, and (ii) a vortex pair.

The theories/...

The theories of Lamb[8] and Squire[9] give the variation of velocity with time for a single vortex as

$$v_t \propto t^{-\frac{1}{2}}$$

The vortex pair cannot be dealt with as conveniently, although some indication of the decay rate is given by a non-rigorous approach used by Flower (unpublished). If the system is assumed to have a constant pattern with, in particular, the position and magnitude of the peak velocity being uniquely related to the distance between vortex cores and the wake drift velocity, then the distance between vortex cores would be expected to be proportional to $t^{\frac{1}{2}}$. The linear momentum of the system would be constant, but would then also be proportional to velocity x time. Hence

$$v_t \propto t^{-1}$$

This approach leads to an inconsistency which suggests that a constant pattern is not in fact possible for a vortex pair, but gives nevertheless some indication of how a vortex pair decays.

Looping at the surface occurred on one test of the rectangular wing at a time when the other tests were undergoing rapid decay. But whether looping occurs or not, the cores must intermix, and the intermixing would be of more significance in influencing the decay rate than the instability phenomenon.

6. CONCLUSIONS

(a) For each wing, the wake drift rate increases with incidence and decreases with increasing core separation.

(b) The onset of appreciable changes in the core separation distance is associated with the transition from one wake pattern where the vortices appear as discrete cores to another where the maximum velocity remains around the wake centre. This occurred at about:

$$25 \text{ s for the elliptic wing}$$
$$60 \text{ s } \text{"} \text{ "} \text{ rectangular wing}$$
$$25 \text{ s } \text{"} \text{ "} \text{ swept wing}$$
$$<5 \text{ s } \text{"} \text{ "} \text{ delta wing}$$

(c) There are two different rates of decay of the peak rotational velocity, v_t. Initially,

$$v_t \propto t^{-\frac{1}{2}}$$

and after a finite transition period,

$$v_t \propto t^{-1} .$$

The transition begins at a time depending on the wing geometry and scale. This time was about:

$$30 \text{ s for the elliptic wing}$$
$$50 \text{ s } \text{"} \text{ "} \text{ rectangular wing}$$
$$20 \text{ s } \text{"} \text{ "} \text{ swept wing}$$
$$10 \text{ s } \text{"} \text{ "} \text{ delta wing.}$$

These are of the same order as the wake age when appreciable changes in core separation begin. The transition is therefore associated with the change in wake pattern.

(d) It is postulated that, in theory, a decay law exists which encompasses all the wings. This is expressed as

$$\frac{v_t b_o{}'}{K} \propto \left(\frac{vt}{b_o{}'^2} \right)^{-c}$$

where the index $c = \frac{1}{2}$ for $\dfrac{vt}{b_o{}'^2} < \tau$,

$$= 1 \text{ for } \frac{vt}{b_o{}'^2} > \tau .$$

τ is some constant whose value was estimated from the data to be between 3×10^{-3} and 6×10^{-3}.

6. (continued)

(e) The development of the wake is described as follows:

The vortices start off as two discrete cores which grow independently of each other and maintain their initial separation. The peak rotational velocity decays as $\text{time}^{-\frac{1}{2}}$.

But they cannot grow indefinitely without coming extremely close to each other. When this happens, at a time which depends on the wing geometry and scale, the cores intermix and the wake system thereafter grows as a pair of interlocked cores, increasing the separation of their centres with time. The maximum velocity decays as time^{-1}.

Their mutual interference may lead later to the formation of clusters of secondary vortices. Looping may occur, but whether loops appear or not, the cores must intermix.

(f) The two parts of the wake development can be represented by two simple flow models:

(i) a single vortex, with solid rotation in the core and potential flow in the surrounding fluid, and

(ii) a vortex pair consisting of two cores descending with constant linear momentum.

(g) The examination of the decay of vortex wakes by the plunging of models into water has proved extremely useful as a means of visualising and understanding the phenomena. The results appear to be in fair agreement with full scale tests, bearing in mind that some differences are to be expected due to the uncertainties of the technique. One such uncertainty is connected with conditions along the length of the vortices - axial flow would not be present on the surface of the water and any effect dependent on axial motion would not be reproduced. Another error could be created if impurities formed a film on the water surface: the precautions taken in the present tests are believed to have been sufficient to make this error negligible, although perhaps some investigation of the effect of impurities would be desirable if further tests are made.

7. RECOMMENDATIONS FOR FURTHER WORK

The following suggestions may be made to improve on the apparatus:

(a) To keep down velocity changes during the travel of the model, a flywheel can be attached to the motor shaft.

(b) Some clutch can be included to disengage and engage the driver pulley on the motor.

(c) Camera "shake" can be eliminated by tying down the camera mount, e.g. a tie can connect it to the wall of the Laboratory.

(c) The model attachment can be remade or corrected to eliminate the slight inclination of the model span to the upper edge of the photograph frame (see Fig. 6).

(e) Pulleys with a larger variety of diameters may be provided to extend the speed range.

Further investigations can include:

(a) The measurement of core radius, suitably defined.

(b) Non-dimensionalizing the wake drift and core separation curves.

(c) Tests with wings of other shapes and scale.

(d) The motion of the wake near ground. A board can be lowered into the tank to simulate the ground.

(e) Studies of the vortex patterns at selected planes inside the water. A slit of light can be reflected across the water inside the tank to illuminate the plane. Flow visualization material, to be useful here, must have the same density as the water.

(f) Checking the non-dimensionalized decay plot by utilising data collected from various other flight experiments.
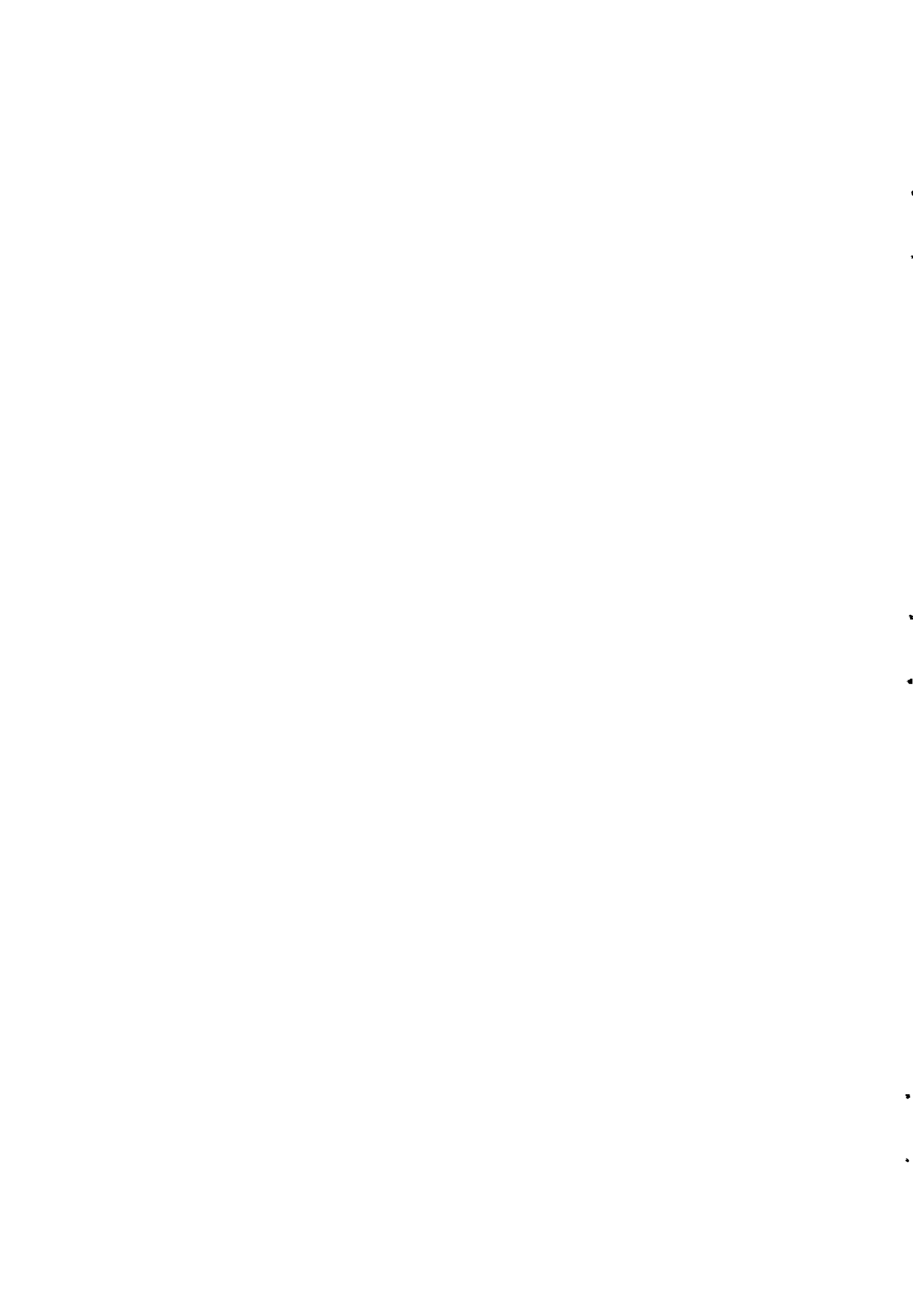
Motion of a Pair of Vortices

The mutually induced velocities of a pair of vortices of unequal circulation will result in some rotation about a centre which is easily calculated.

Consider two vortices of circulations K_1, K_2 (where $K_1 > K_2$), separated by a distance b'.

Fig. A shows the directions of the mutually induced velocities when the vortices rotate in (a) opposite senses and (b) the same sense. If x is the distance of K_1 from the centre of rotation, O, then

$$x_{opposite} = \left(\frac{K_2}{K_1 - K_2} \right) b' \quad ,$$

and

$$x_{same} = \left(\frac{K_2}{K_1 + K_2} \right) b' \quad .$$

Fig. B shows the pattern of streamlines of the flow between the vortices. The distance of the stagnation point in (b) from K_2 is in fact equal to x_{same}.
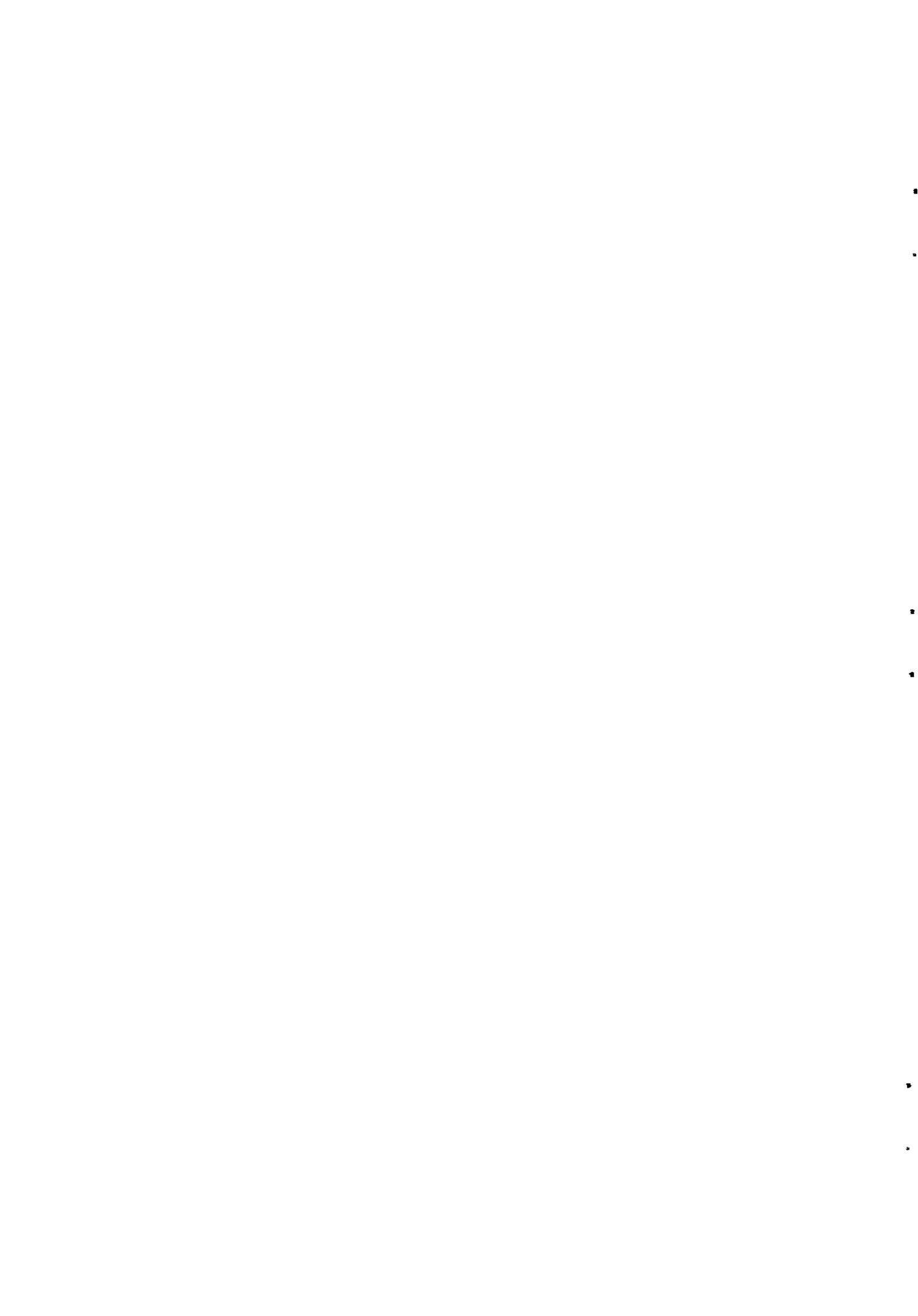
Effect of Wall of Tank on Motion of Vortices

A pair of vortices formed in the water bounded by the cylindrical wall of the tank produces images whose positions are determined by the properties of inverse points[19]. Thus, in Fig. C, $OV_p \cdot OI_p = OV_s \cdot OI_s = R^2$.

The interaction of the vortices with the images thus mars an exact representation of vortex wake motion in an infinite fluid, such as would be practically obtained for vortices shed from high-flying aircraft.

However, if the vortex separation, b', is small compared with the diameter of the tank, the effect of the images would be expected to be pronounced only if the vortices were near the wall. This is the situation obtained in the tests when the model is plunged in close to the wall.

Figure D illustrates this situation and indicates the directions of the velocities induced on vortex B by the other vortex A and the images, C and D.

From the diagram,

$$\theta = \tan^{-1} \frac{b'}{2(R-z)} \qquad ;$$

$$OA = (R-z) \sec \theta \qquad ;$$

$$AC = \frac{R^2}{OA} - OA \qquad ;$$

$$BC = (AC^2 + b'^2 + 2 \cdot AC \cdot b' \sin \theta)^{\frac{1}{2}} \qquad ;$$

and

$$\alpha = \sin^{-1} \left(\frac{AC}{BC} \cos \theta \right) \qquad .$$

The velocity of vortex B in the z-direction is then

$$\dot{z} = \frac{K}{2\pi} \left[\frac{1}{b'} - \frac{\cos \alpha}{BC} - \frac{\sin \theta}{AC} \right] \qquad ,$$

and in the y-direction

$$\dot{y} = \frac{K}{2\pi} \left[\frac{\sin \alpha}{BC} - \frac{\cos \theta}{AC} \right]$$

(cf. in infinite fluid, $\dot{z} = \frac{K}{2\pi b'}$, $\dot{y} = 0$.)
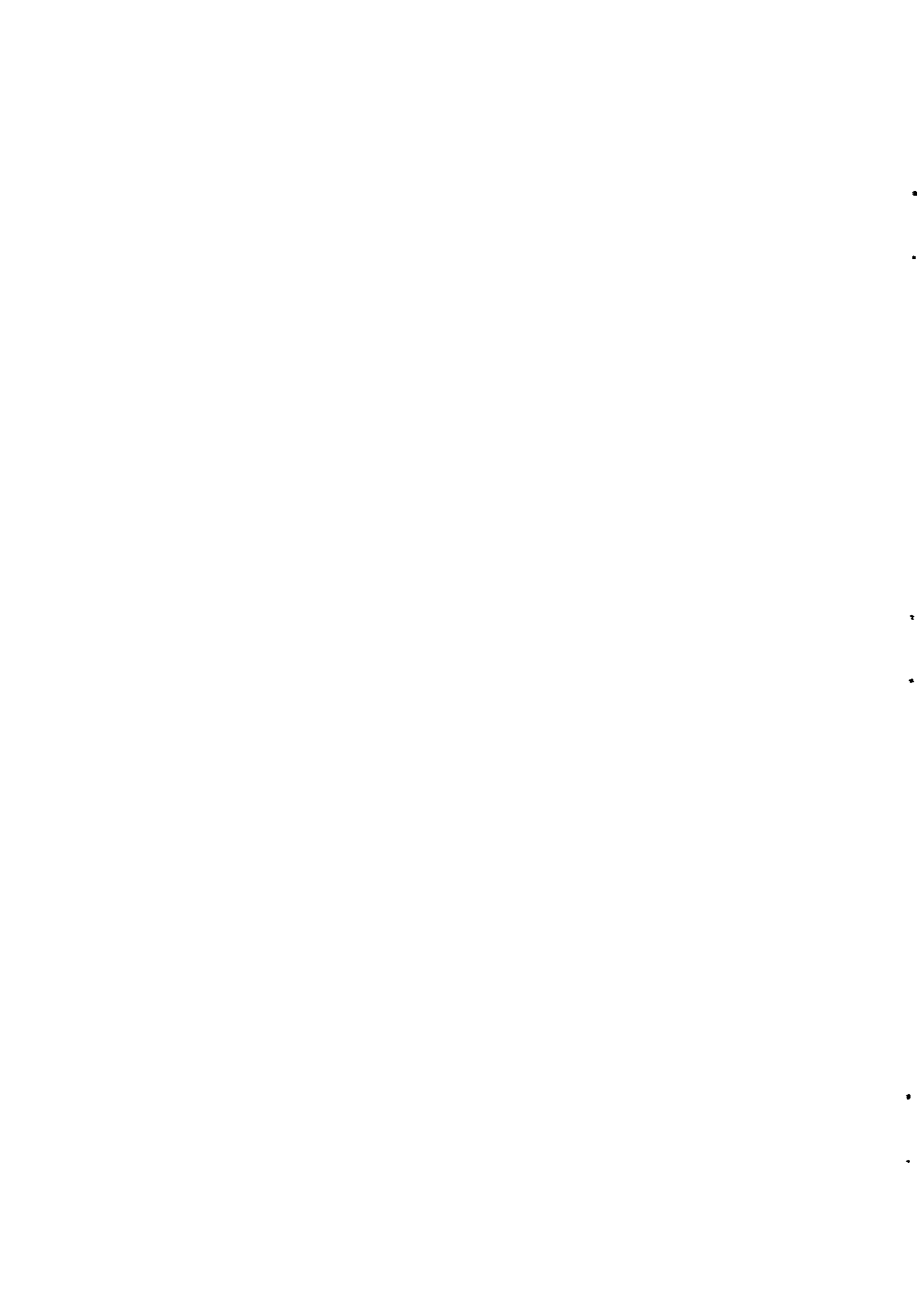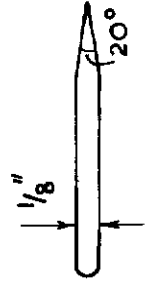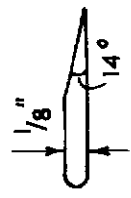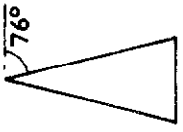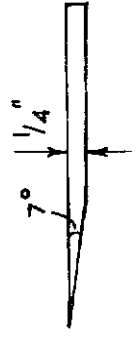
REFERENCES

No.	Author(s)	Title, etc.
1	A. S. Carten, Jr.	Warning : wakes. Astronautics & Aeronautics, Vol.8, No.4, pp.76-81. April, 1970.
2	-	F A A vortex concern mounting. Aviation Week & Space Technology, Vol.92, No.21, p.31. 25th May, 1970.
3	J. W. Wetmore and J. P. Reeder	Aircraft vortex wakes in relation to terminal operations. NASA TN D-1777. April, 1963.
4	D. R. Andrews	A flight investigation of the wake behind a Meteor aircraft and some theoretical analysis. ARC CP 282. December, 1954.
5	C. C. Kraft, Jr.	Flight measurements of the velocity distribution and persistence of the trailing vortices of an airplane. NACA TN 3377. March, 1955.
6	C. B. Millikan	Aerodynamics of the airplane. John Wiley & Sons, Inc., pp.28-65. 1941.
7	J. R. Spreiter and A. H. Sacks	The rolling up of the trailing vortex sheet and its effect on the downwash behind wings. Jour. Aero. Sci., Vol.18, No.1, pp.21-32, 72. January, 1951.
8	H. Lamb	Hydrodynamics. Cambridge University Press, p.592, 6th ed. 1932.
9	H. B. Squire	The growth of a vortex in turbulent flow. The Aeronautical Quarterly, Vol.XVI, Part 3, pp.302-306. August, 1965.
10	T. H. Kerr and F. W. Dee	A flight investigation into the persistence of trailing vortices behind large aircraft. ARC CP 489. September, 1959.
11	R. Rose and F. W. Dee	Aircraft vortex wakes and their effects on aircraft. ARC CP 795. December, 1963.

REFERENCES
(continued)

No.	Author(s)	Title, etc.
12	G. K. Mather	A note on some measurements made in vortex wakes behind a DC-8. National Research Council of Canada, Report No. DME/NAE 1967 (2), Ottawa (1967).
13	F. W. Dee and O. P. Nicholas	Flight measurements of wing tip vortex motion near the ground. ARC CP 1065. 1968.
14	P. L. Bisgood, R. L. Maltby and F. W. Dee	Some work on the behaviour of vortex wakes at the Royal Aircraft Establishment. Unpublished MOD(PE) Material. 1970.
15	-	Royal Aeronautical Society Data Sheets Wings 01.01.01 and 01.01.05.
16	I. H. Abbott and A. E. Von Doenhoff	Theory of wing sections. McGraw-Hill Book Co., Inc., New York, p.16. 1949.
17	B. E. G. Shears and S. G. Shepherd	Low speed characteristics of double-delta wings. University of Bristol, Department of Aeronautical Engineering, B.Sc. Thesis. June, 1967.
18	L. M. Milne-Thomson	Theoretical hydrodynamics. MacMillan & Co. Ltd., London. p.321, 2nd ed. 1949.
19	W. J. Duncan, A. S. Thom and A. D. Young	An elementary treatise on the mechanics of fluids. Edward Arnold Ltd, London. p.111. 1960.

Wing	Planform	Span (in)	Mean chord (in)	Aspect ratio	Wing area (in²)	a_1 (per°) (1)	a_1 (per°) (2)	Section
ELLIPTIC	(ellipse)	6·0	1·57	3·82	9·42	0·052	0·052	1/8″ 20°
RECTANGULAR	(rectangle)	10·0	1·0	10·0	10·0	0·065	0·061	1/8″ 14°
SWEPT	(swept, 30°)	6·0	1·5	4·0	9·0	0·045	0·044	As elliptic
DELTA	(delta, 76°)	4·5	4·5	1·0	22·5	0·017	0·018	7° 1/4″

NOTES

(1) R Ae S Data sheets[15] For $Re = 2 \times 10^4$, $a_0 \simeq 0.77$ per°

(2) Formula in Abbott & von Doenhoff, "Theory of wing sections"[16] same a_0

Table 1.   Wing data

Rig

I — 4 Guides
A — C Pulley release
          mechanism

Micro-
switches

Camera

Electric
motor

C

Spotlight

3

A

4 B

Elevated floor

Model

Mirror

Clock

Graduated scale

Tank
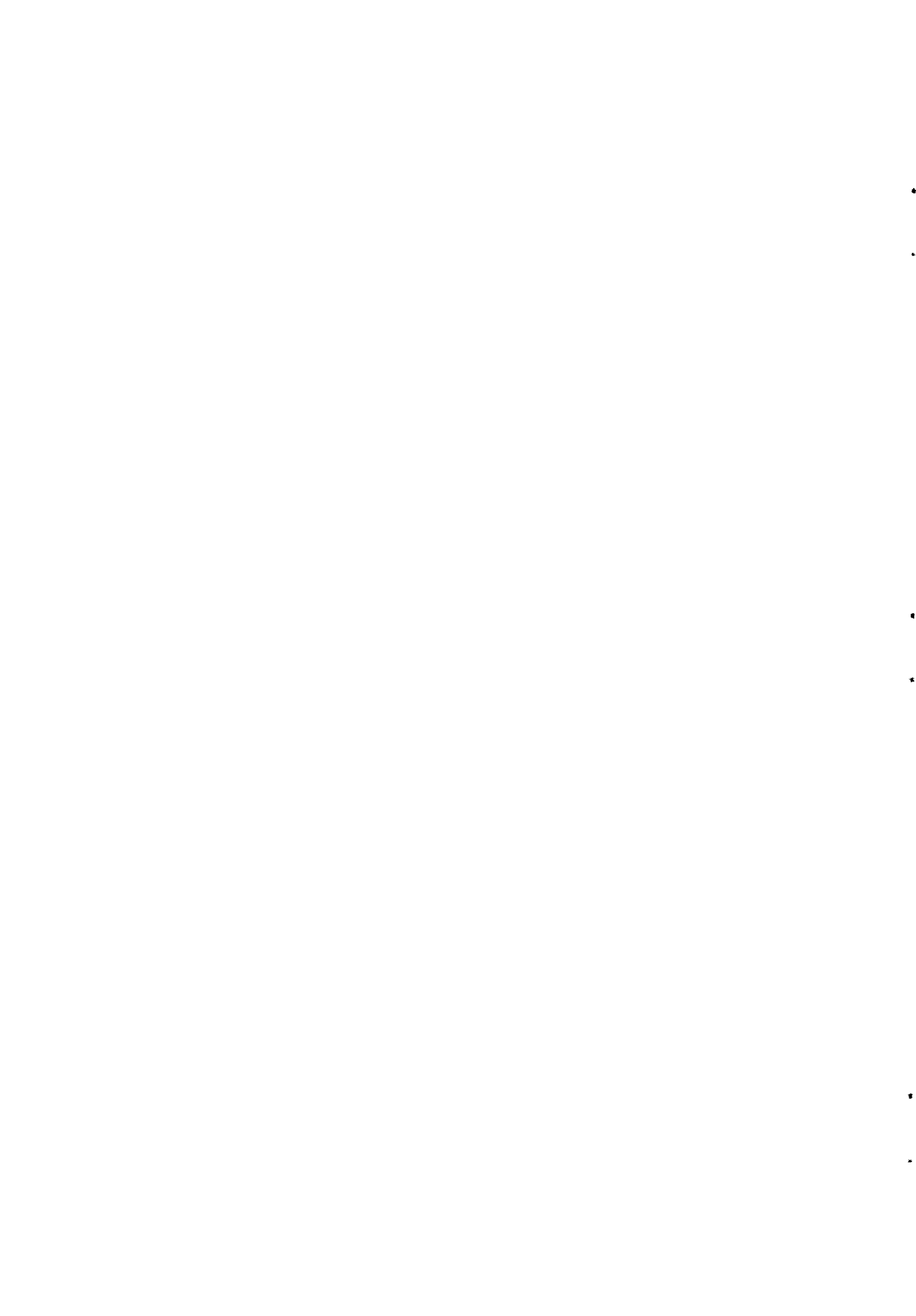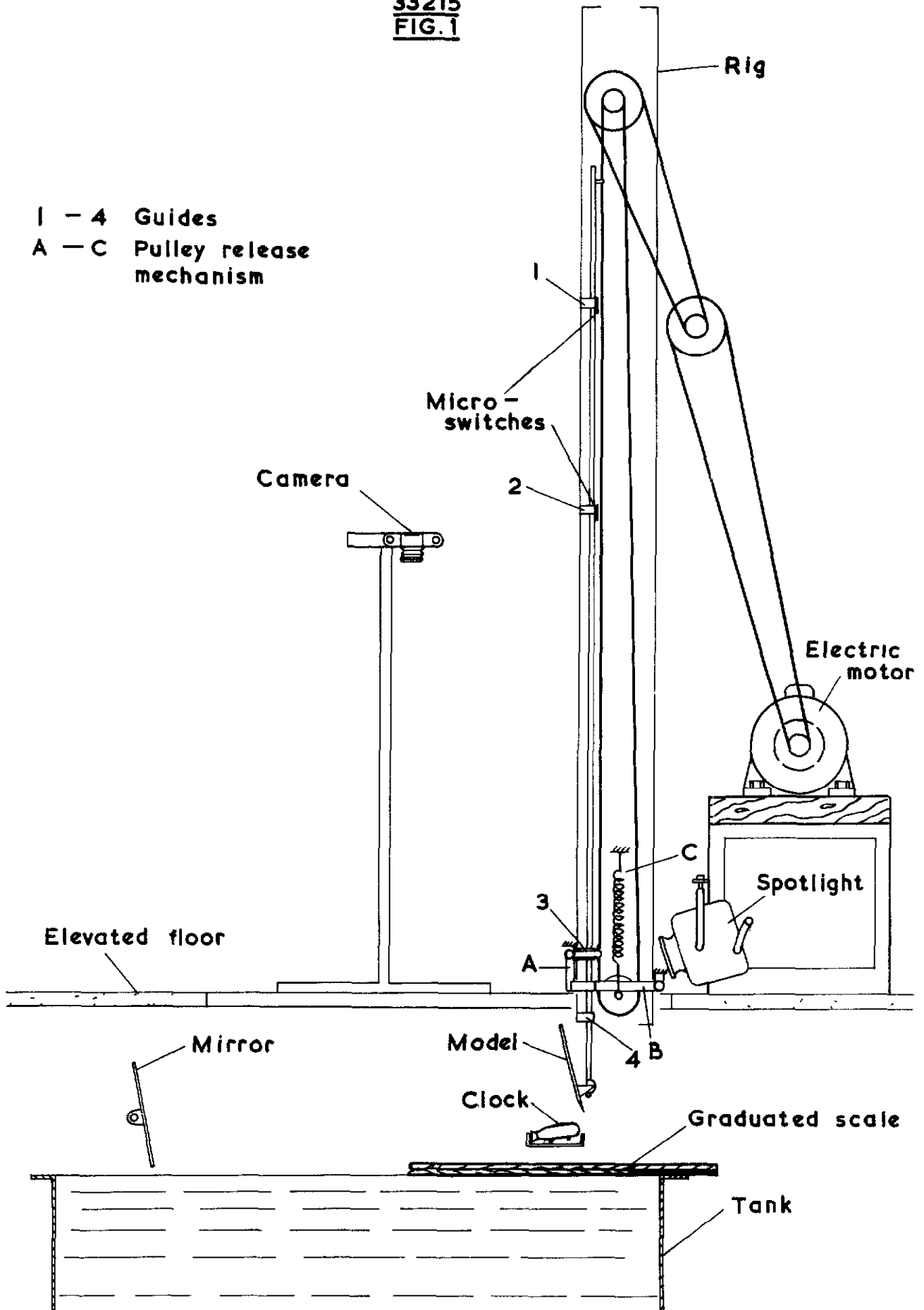
Diagram of apparatus
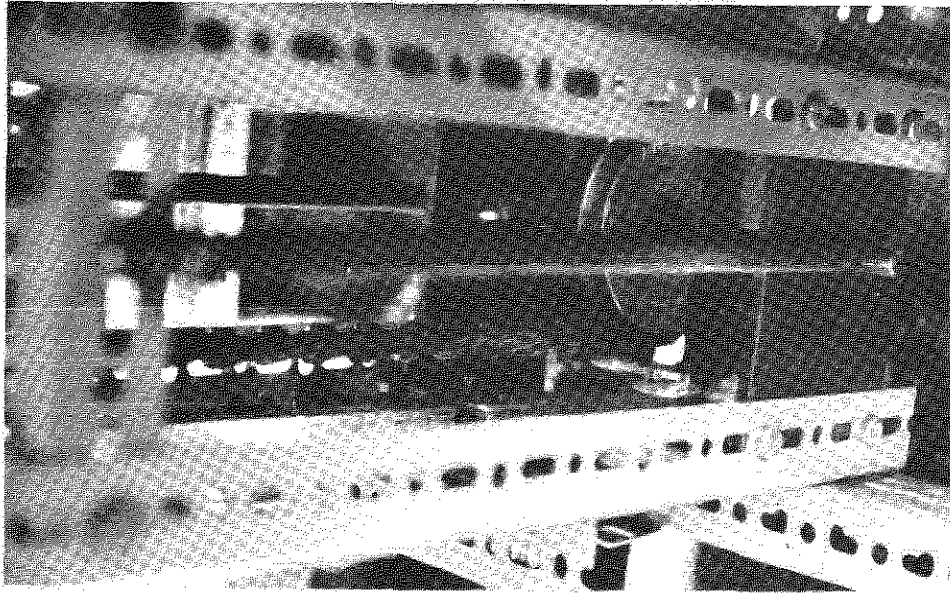
FIG.3. Pulley release mechanism.
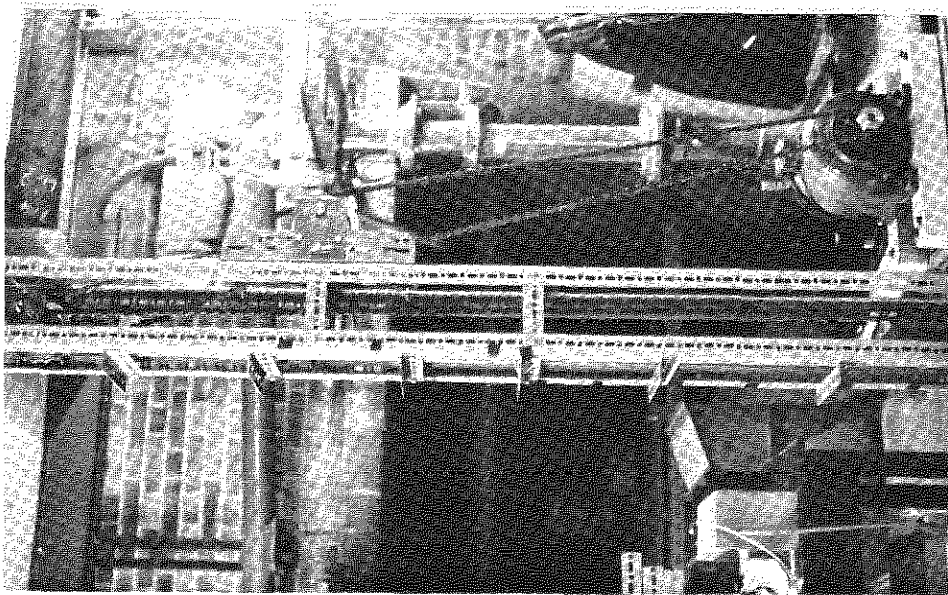
FIG.2. The rig.
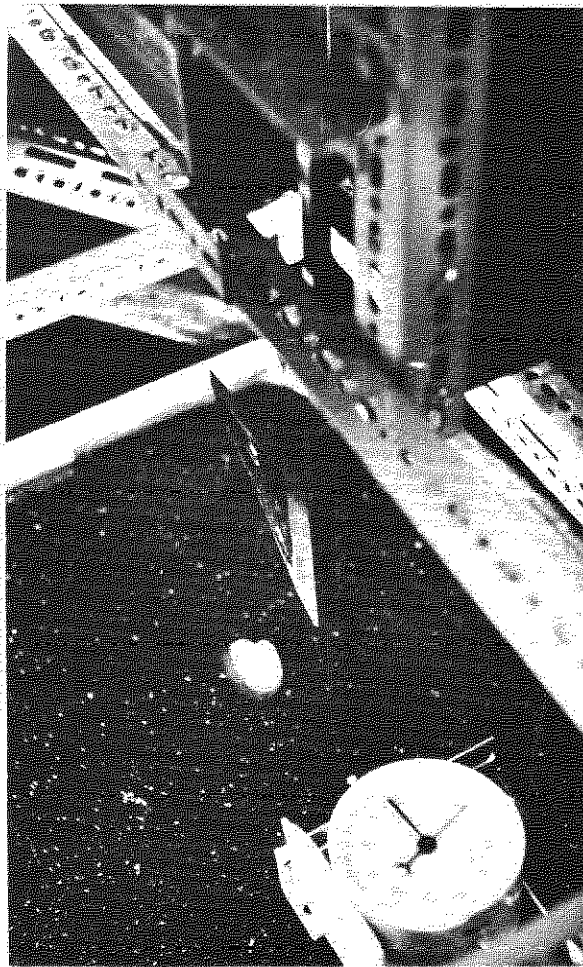
Model poised for plunge (clock in foreground and graduated scale in background).
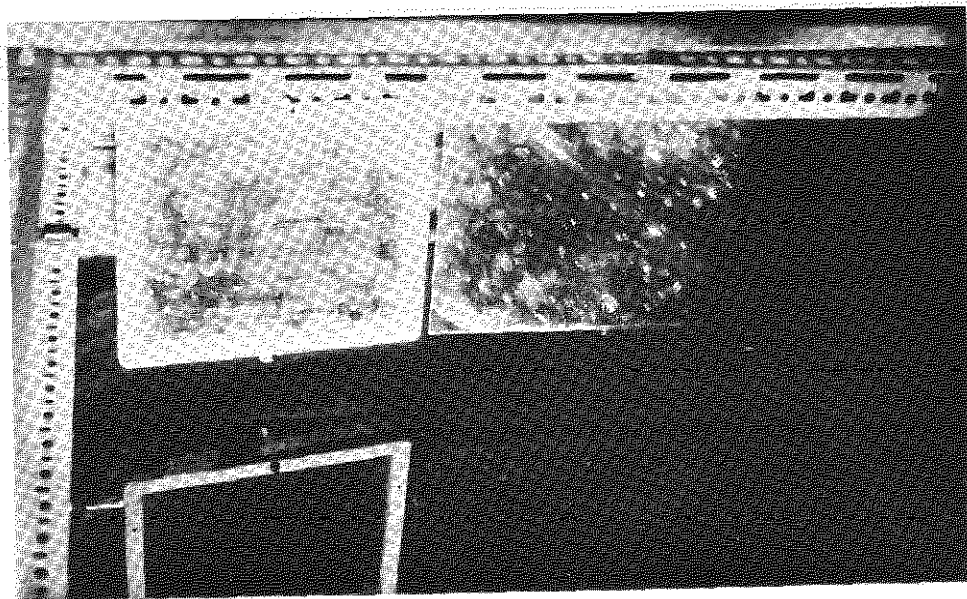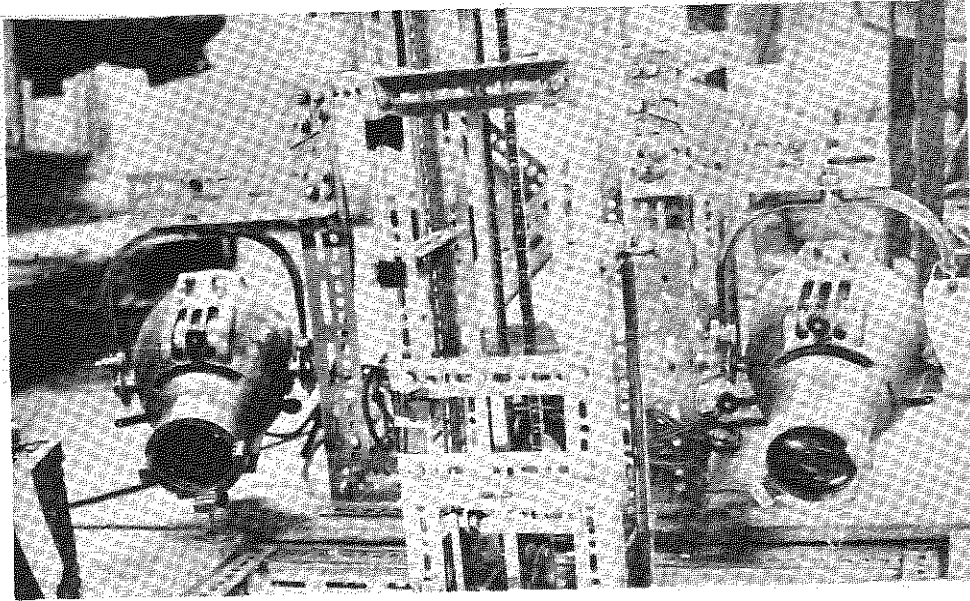
Spotlights and mirrors

Field of view of mounted camera, showing to good advantage size of model delta wing, and positions of clock and scale.
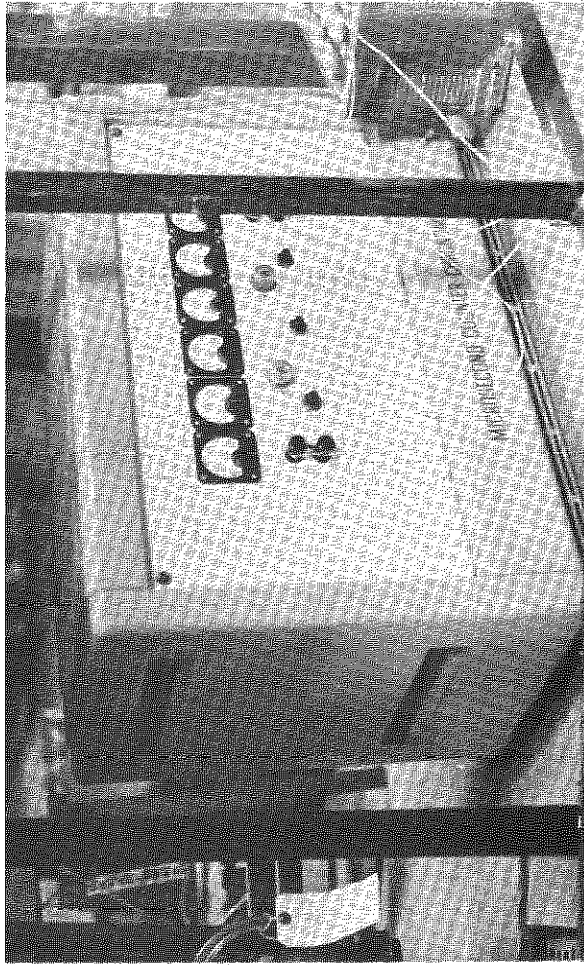
Microswitches and chronometer
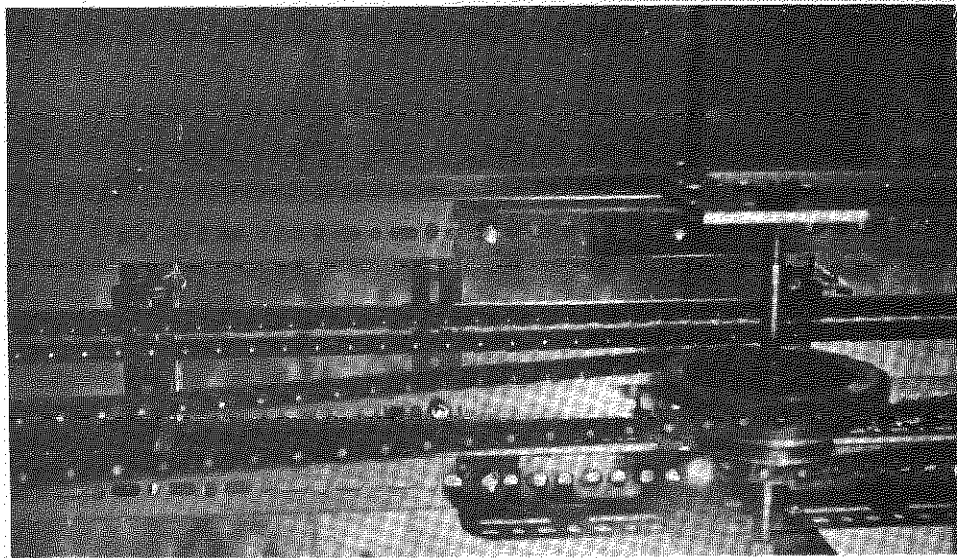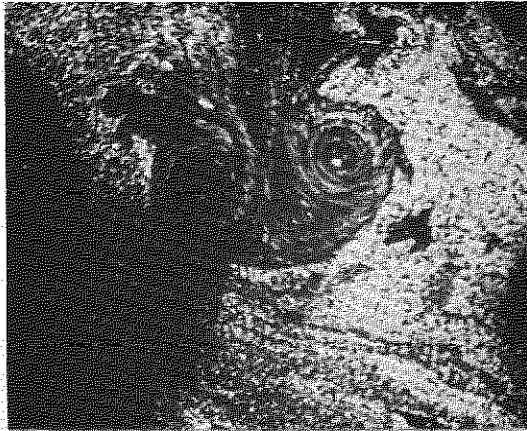
(a) Lycopodium powder
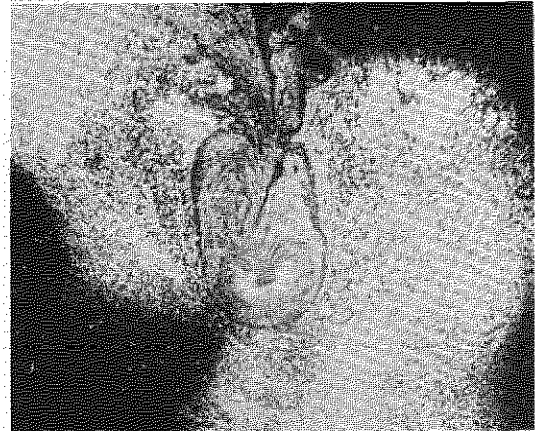
(b) Lycopodium, looping at surface
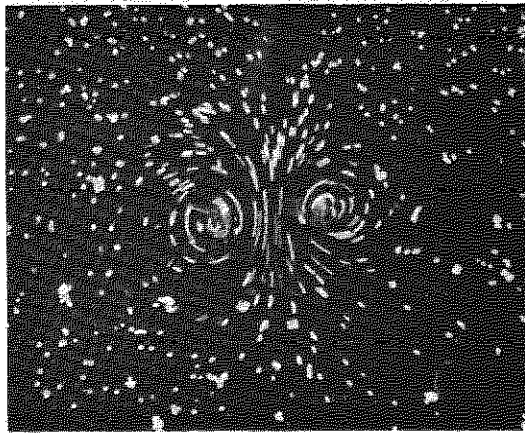
(c) Paper punchings from data tape
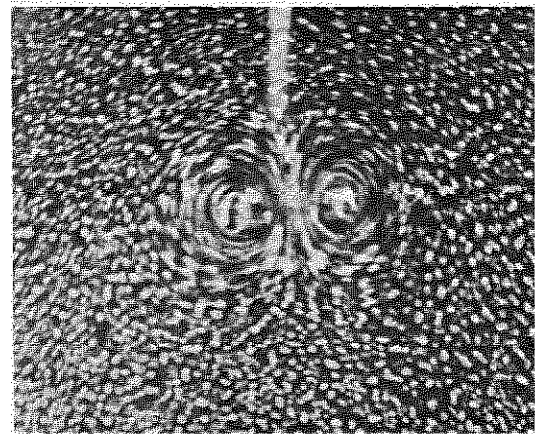
(d) Sawdust

(e) Aluminium powder

Flow visualisation tests

33215
FIG. 9.

t (s)
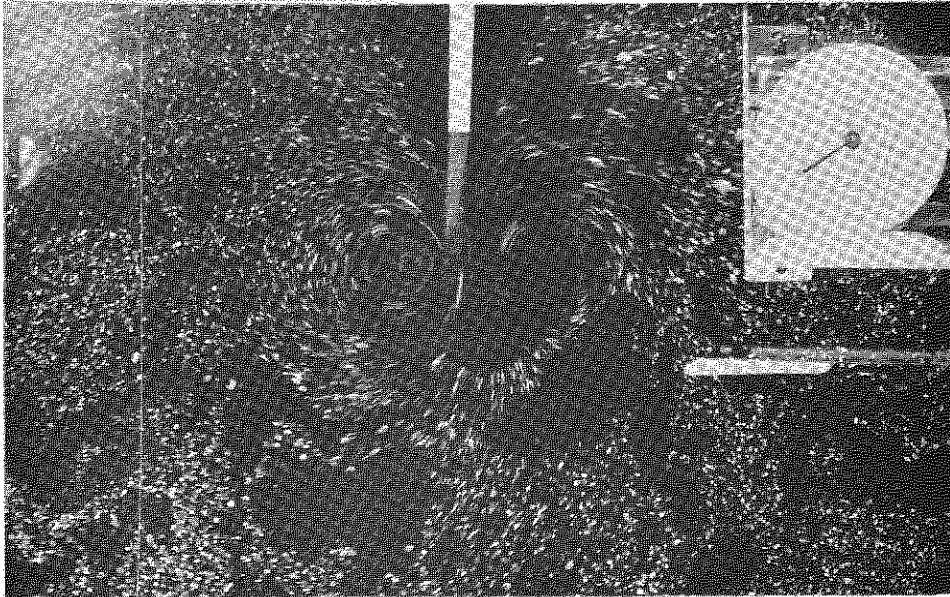
4
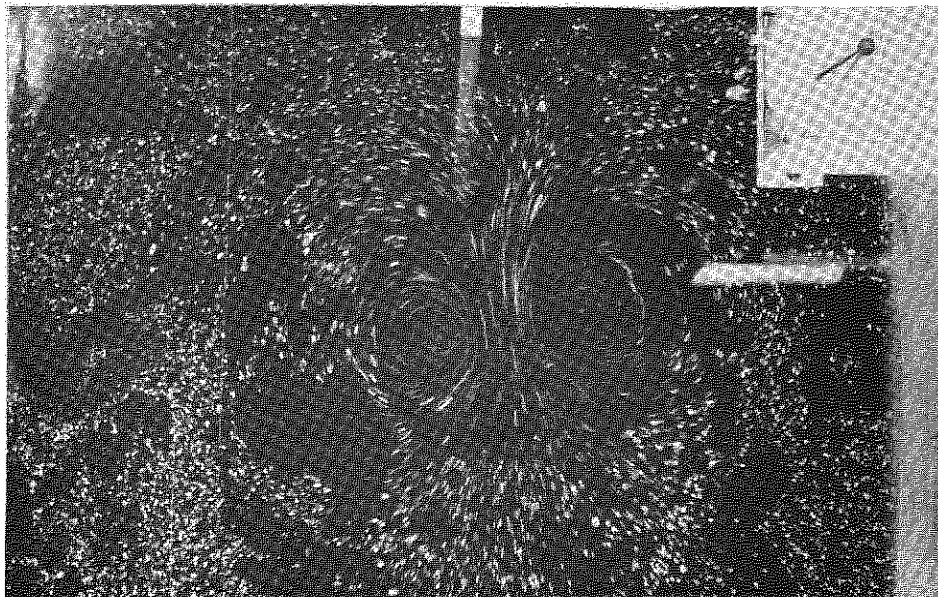
11
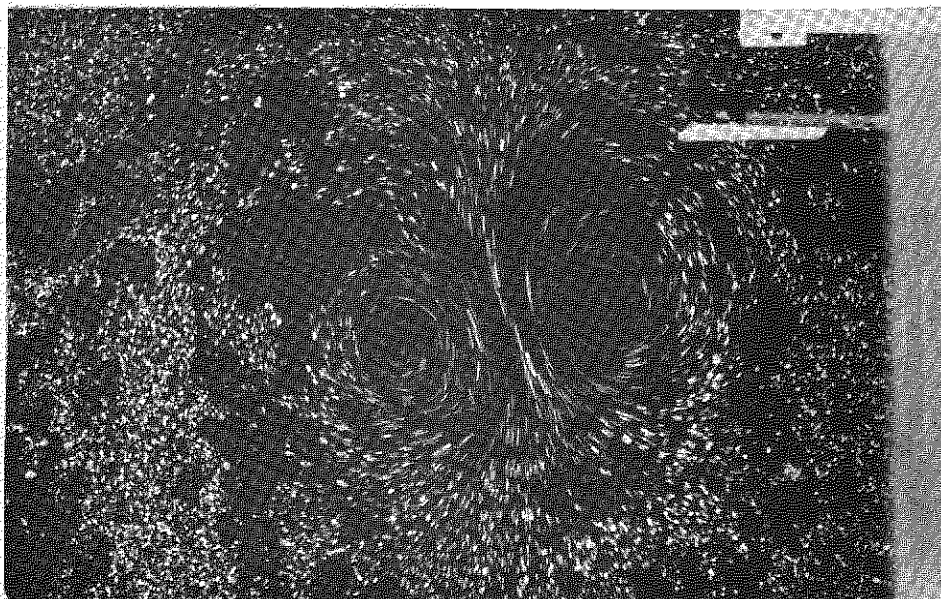
18

Wake patterns: elliptic wing, $\alpha = 12°$, U=2·0 ft/s

t (s)

35·5

½ s exp.

1 s exp

53

82

FIG. 9 (contd.)

t(s)

7

19

27·5
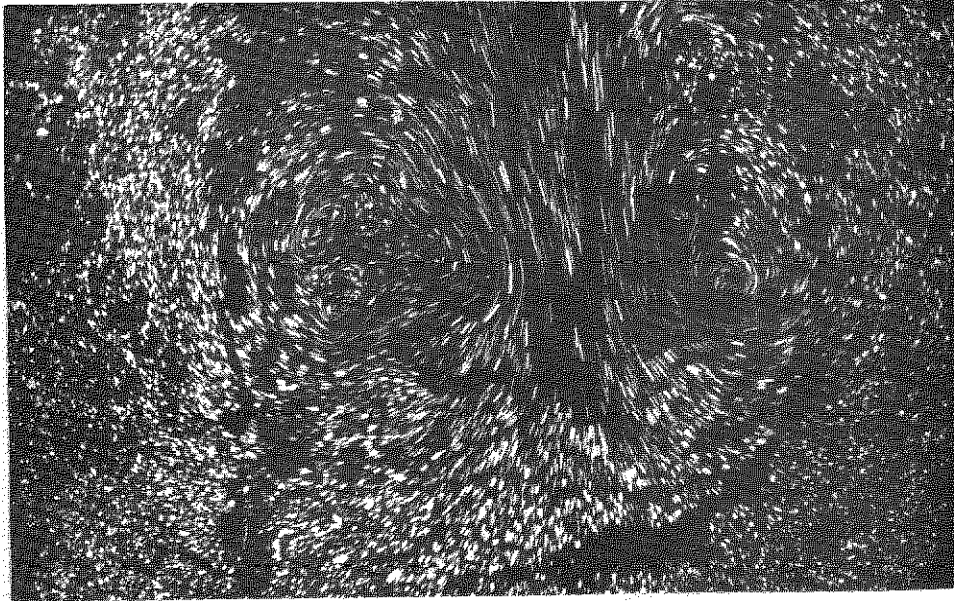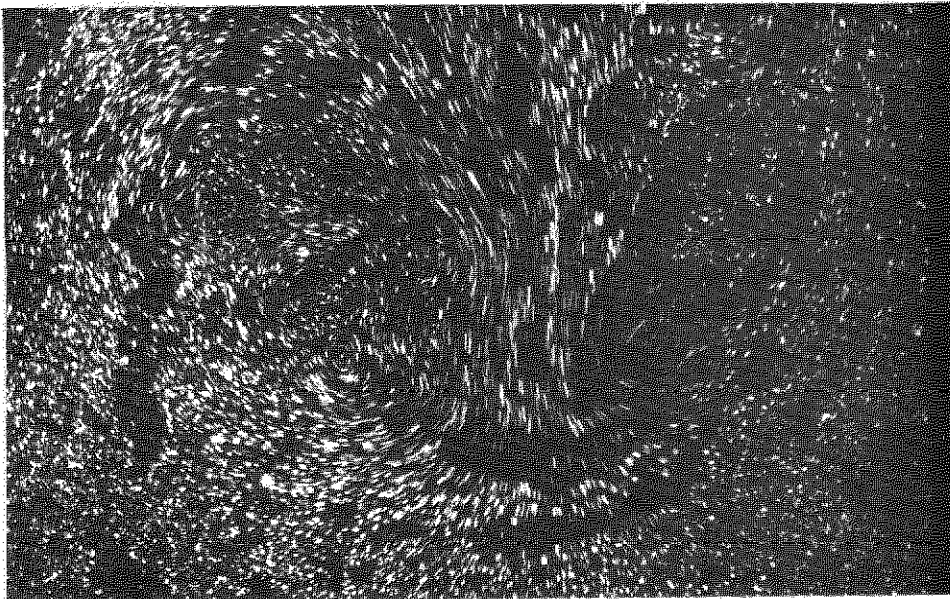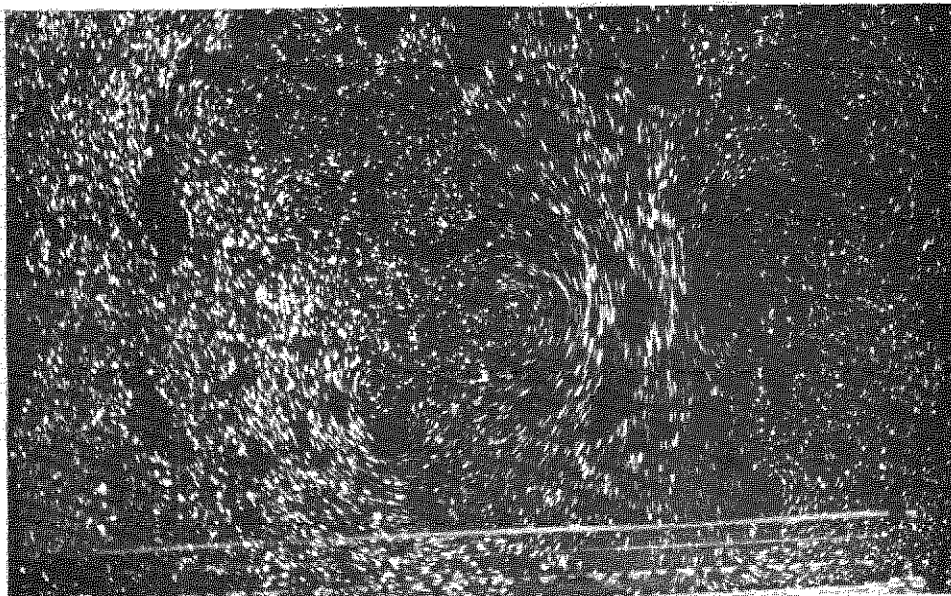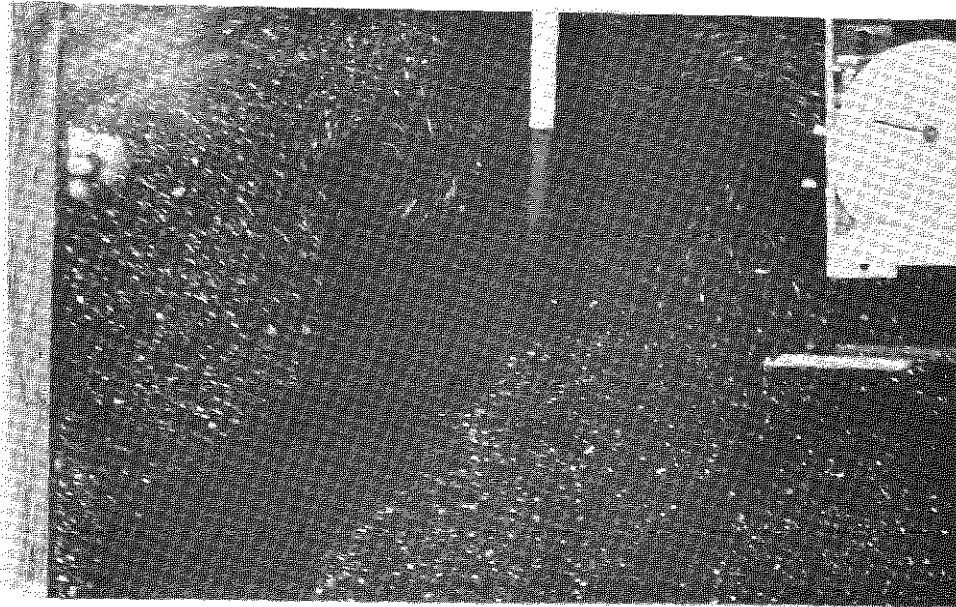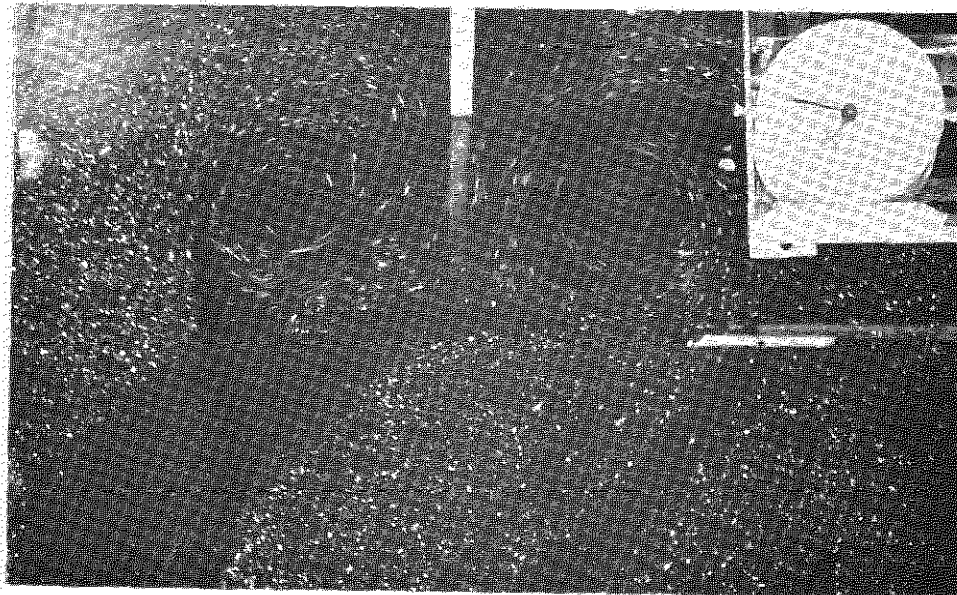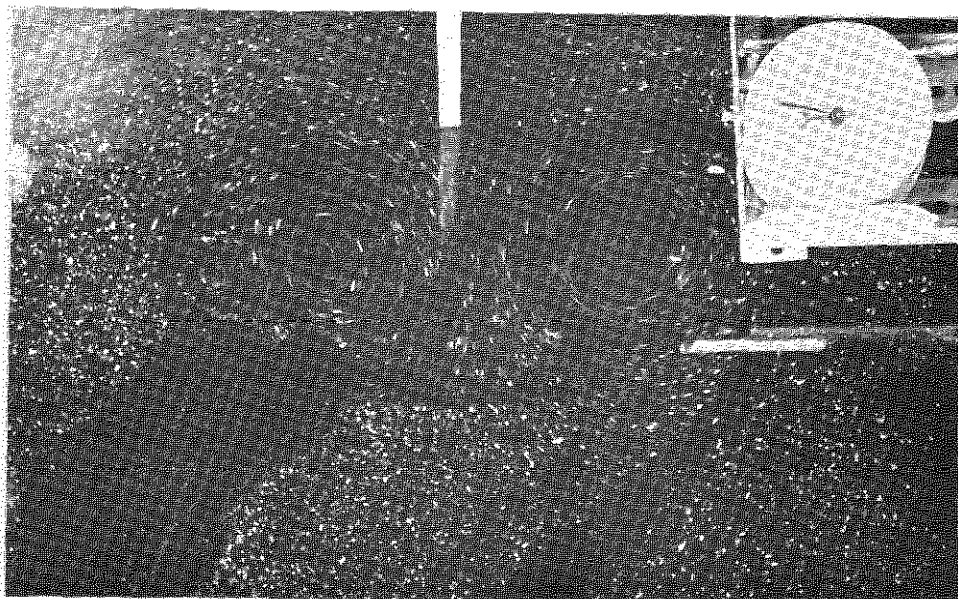
½ s exp.

Wake patterns: rectangular wing, $\alpha = 5°$, $U = 3.0$ ft/s

1 s exp.

t (s)
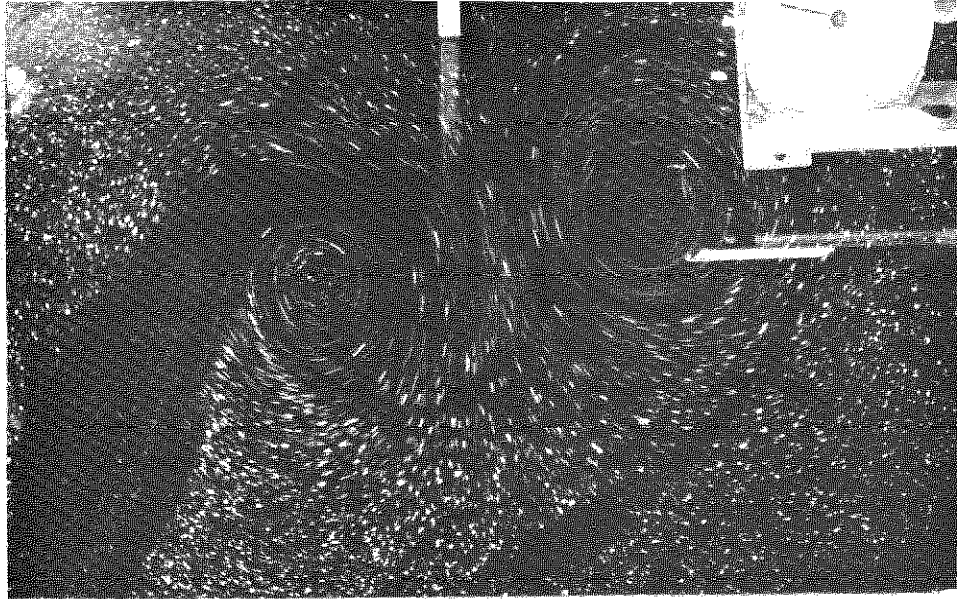
44

72

131

FIG. 10 (contd.)

t (s)

4

9
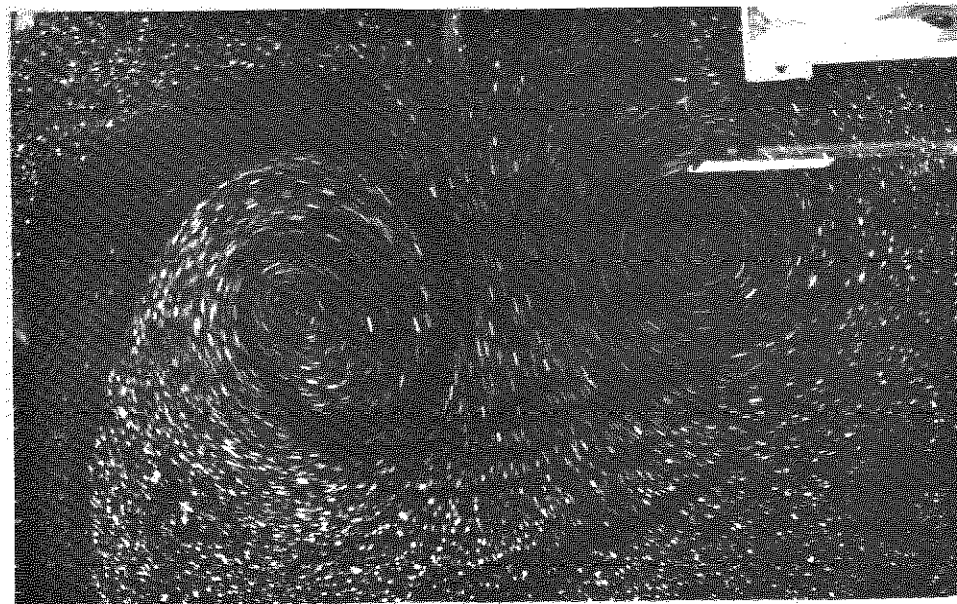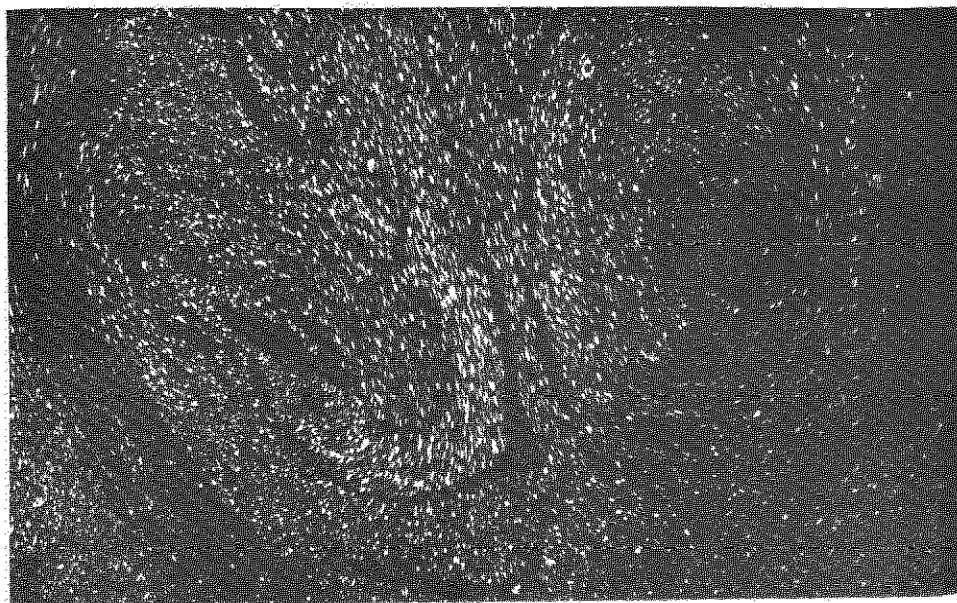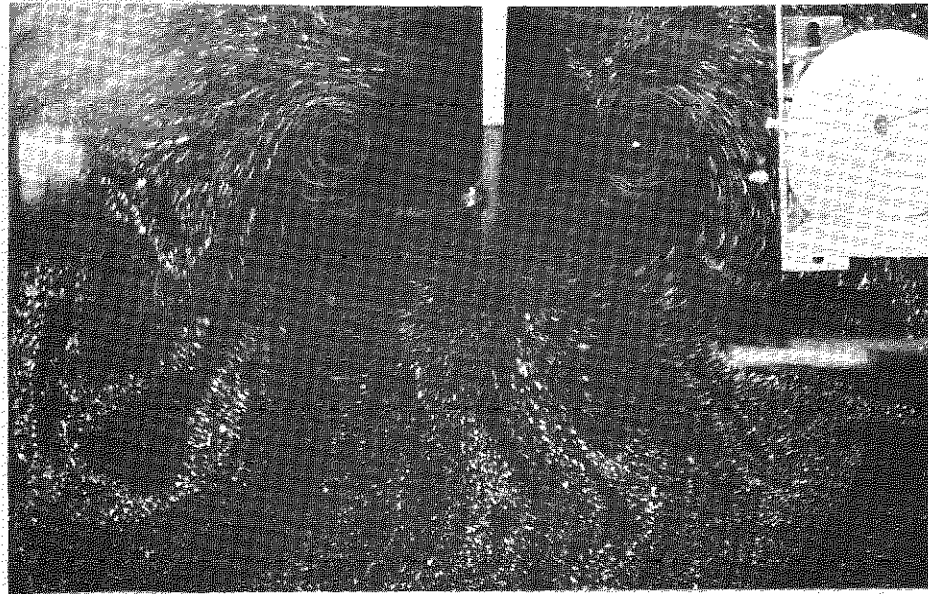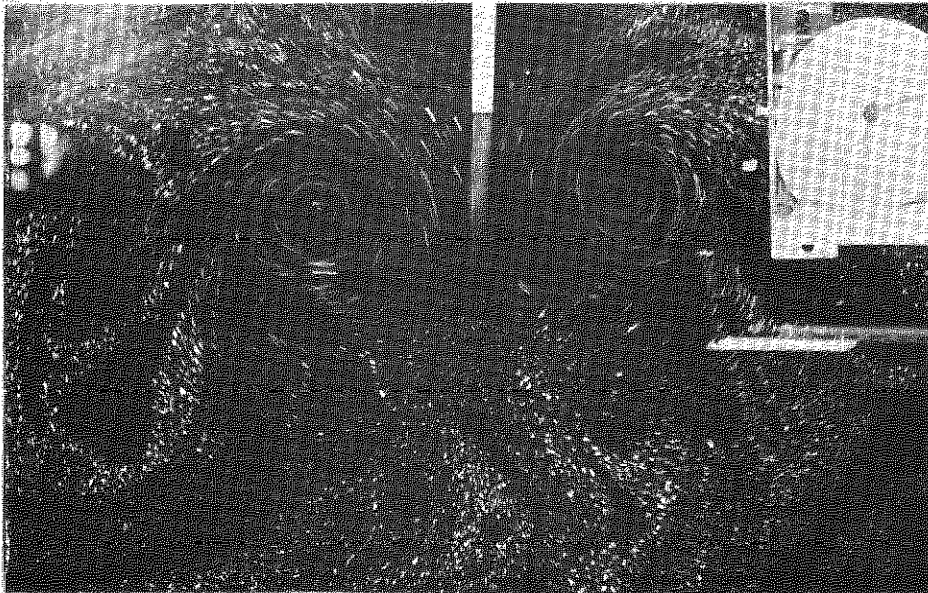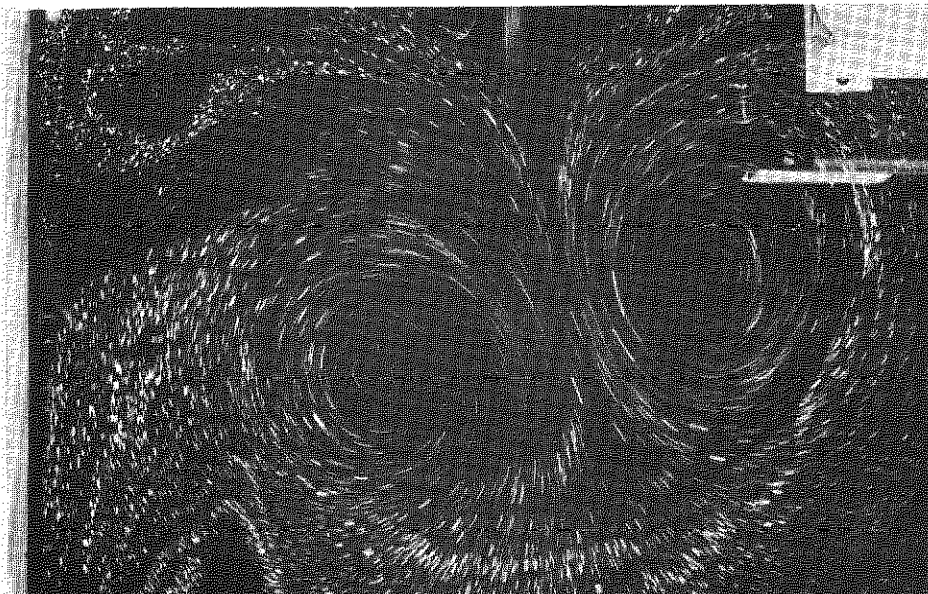
½ s exp

1 s exp.

38

Wake patterns: rectangular wing, $\alpha = 10°$, U = 2.2 ft/s

t(s)

70

106

140

FIG. 11. (contd.)

t (s)

4·5

18·5
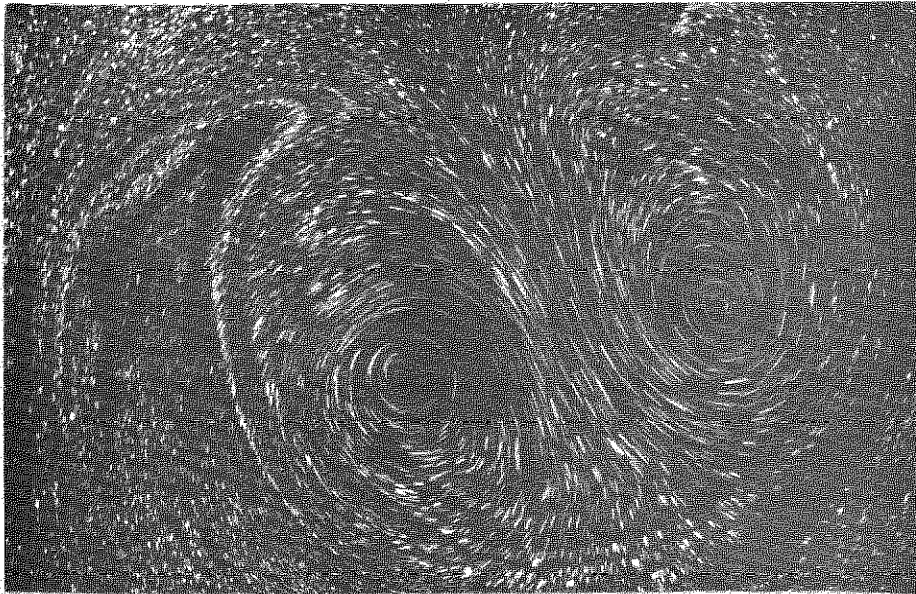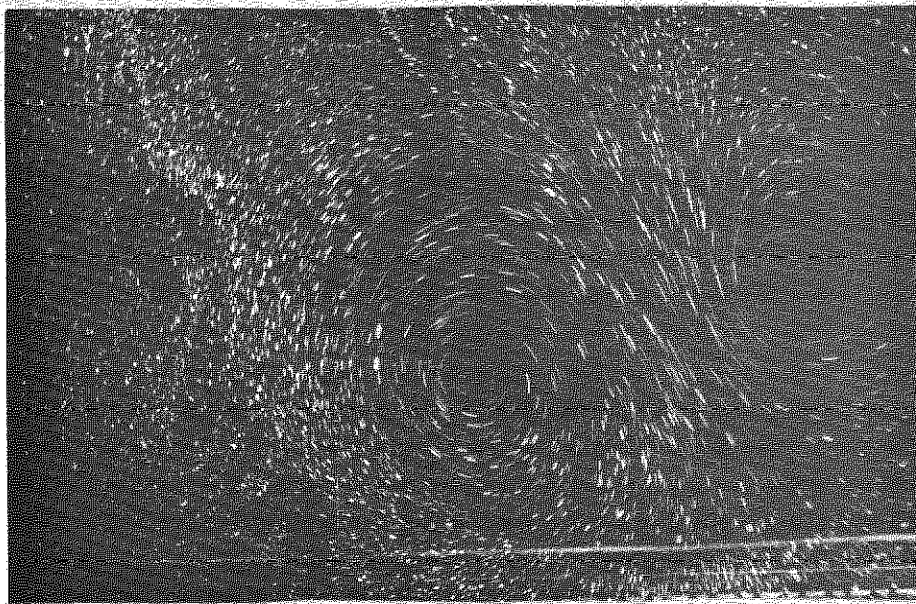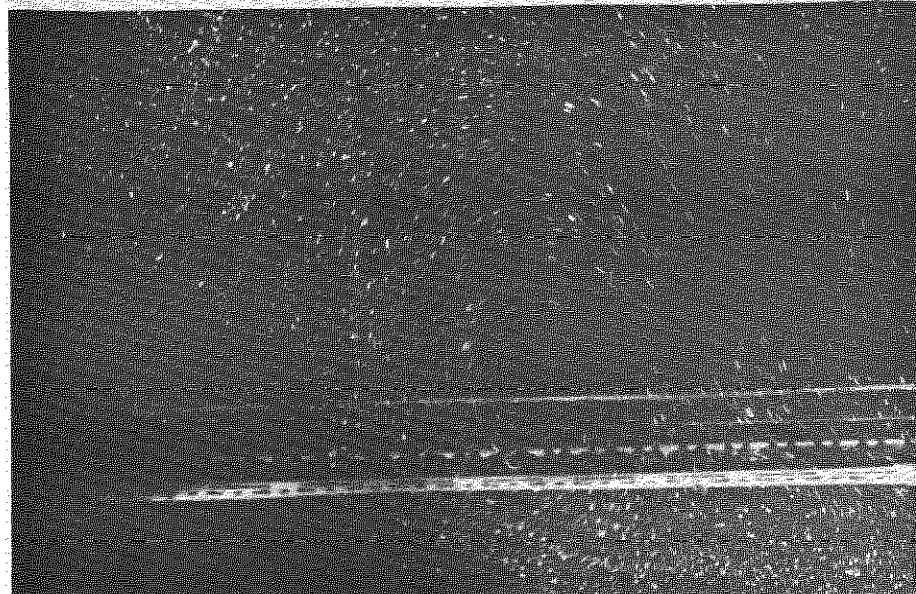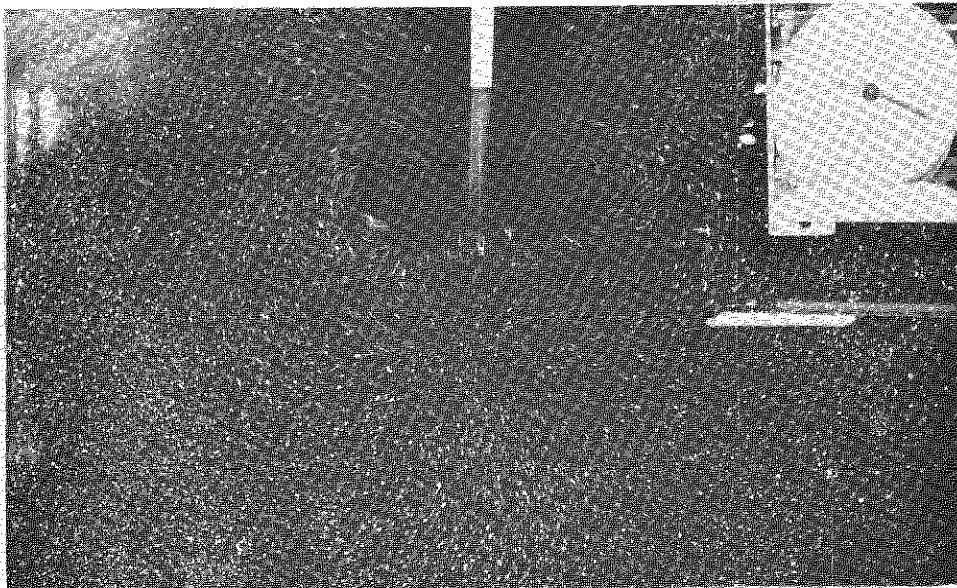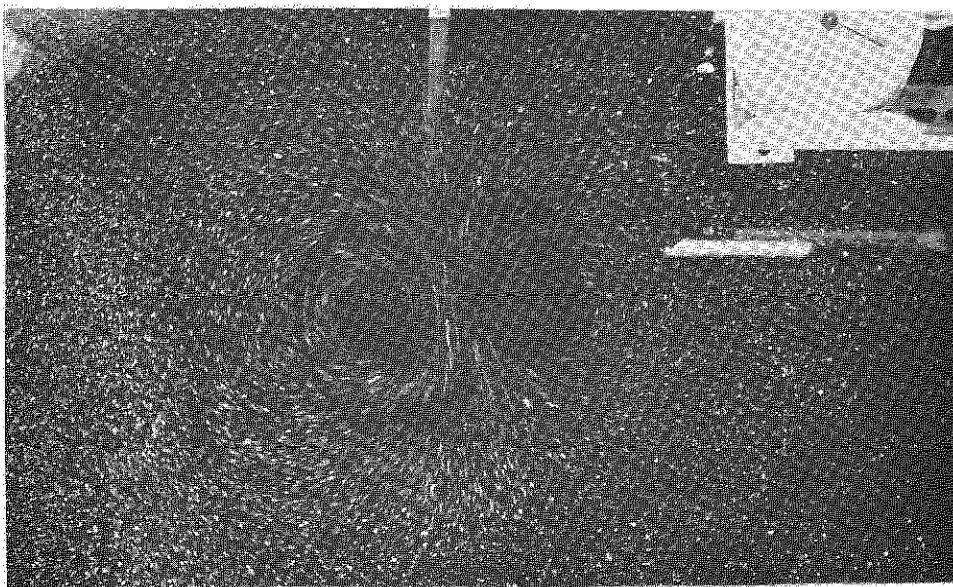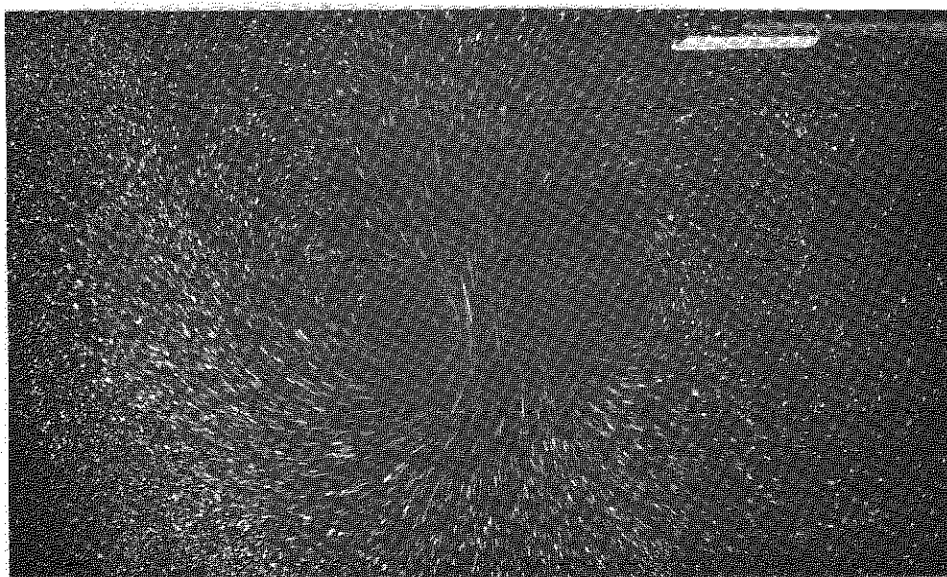
½ s exp.

1 s exp.

35·5

Wake patterns: swept wing, $\alpha = 12°$, U = 2·0 ft/s

FIG. 12. (contd.)

t (s)

O

4·5

9·5
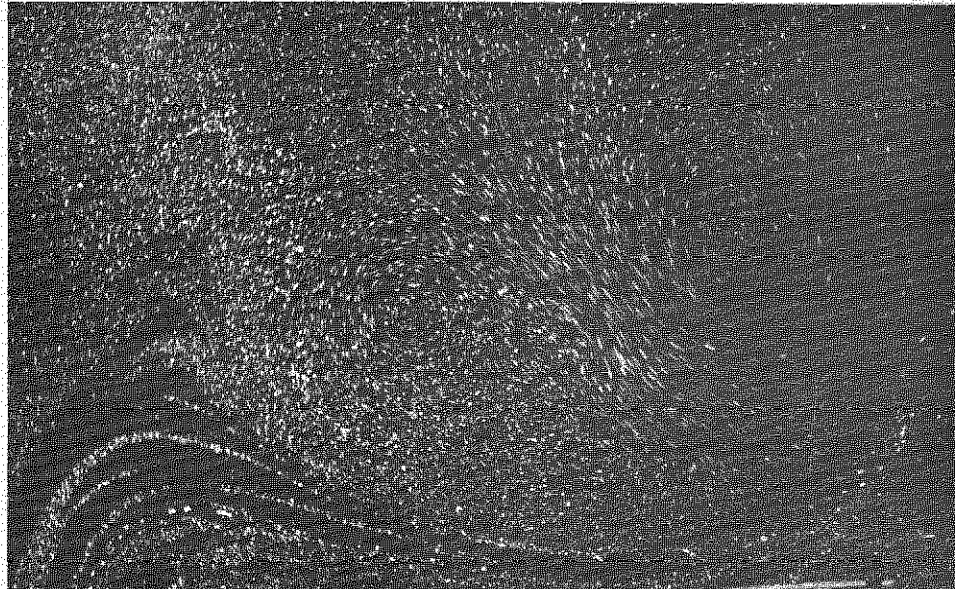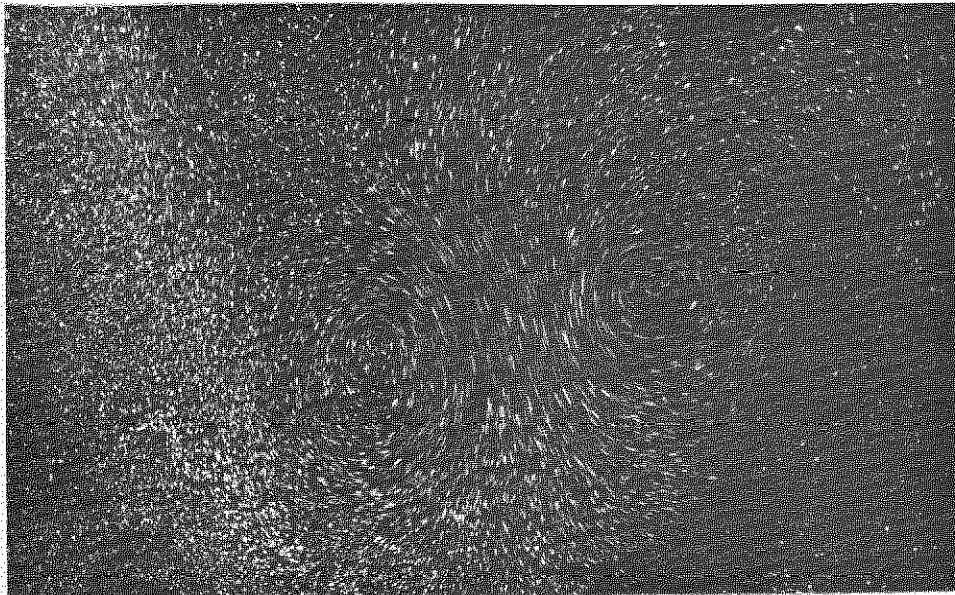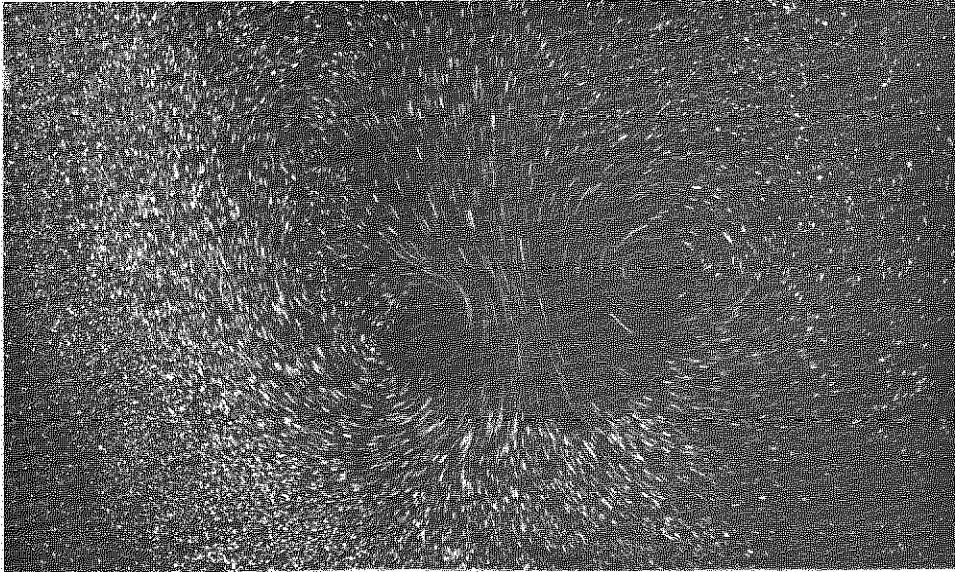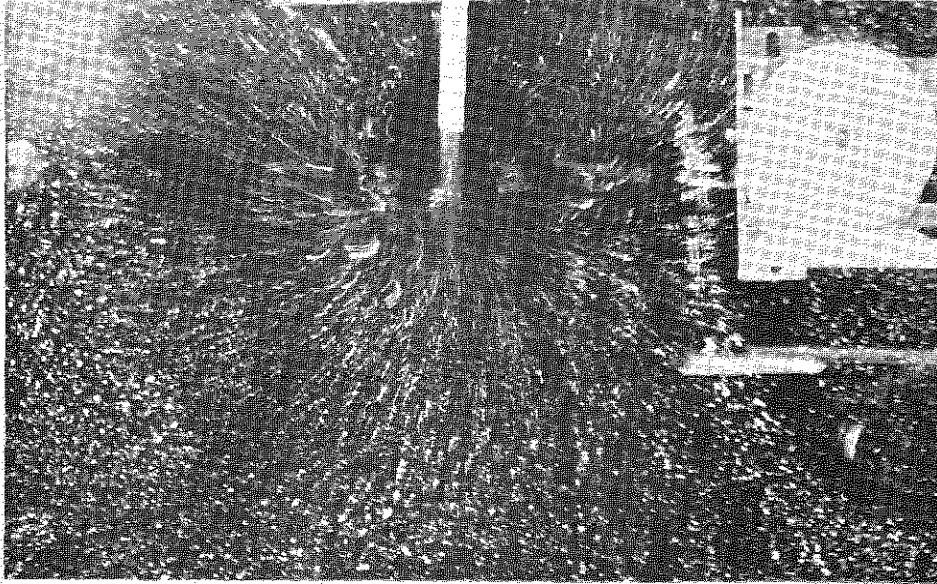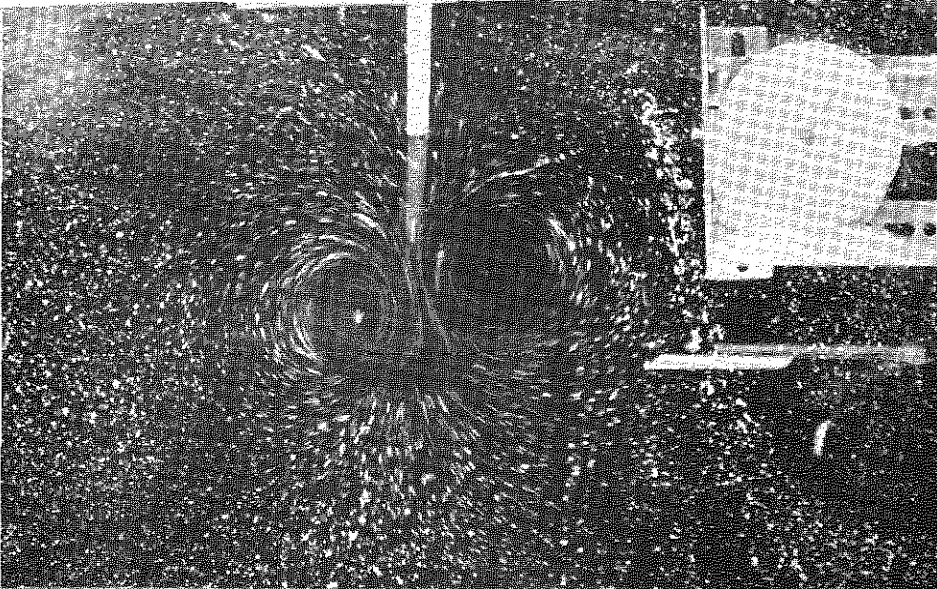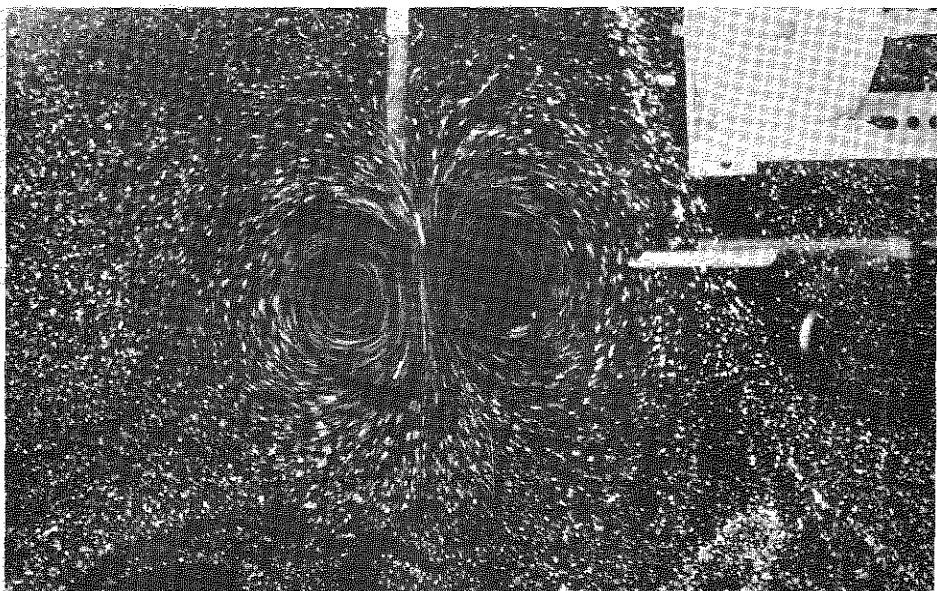
½ s exp.

Wake patterns: delta wing, $\alpha = 5°$, U = 2·6 ft/s

1 s exp.

t (s)

20

27

40

FIG. 13. (contd.)
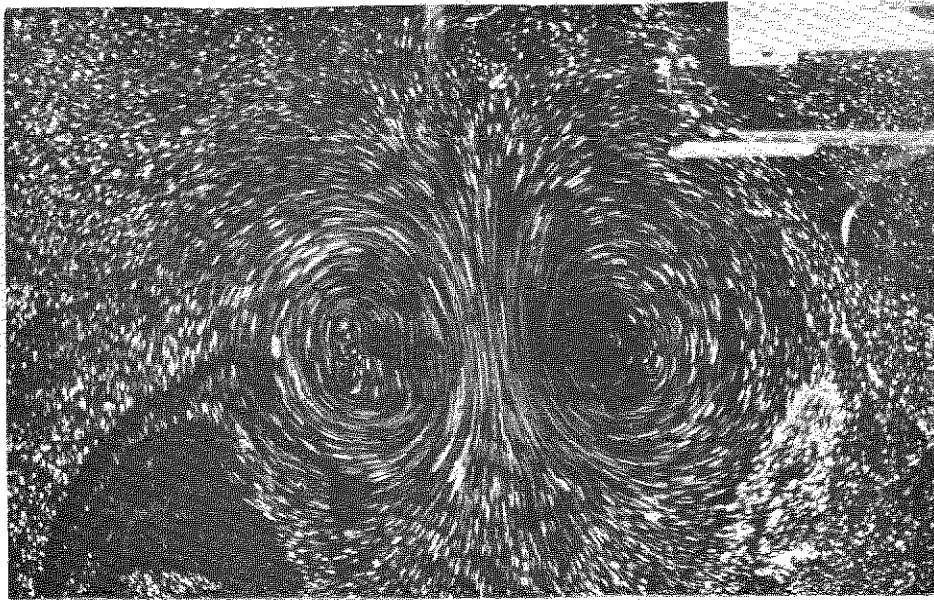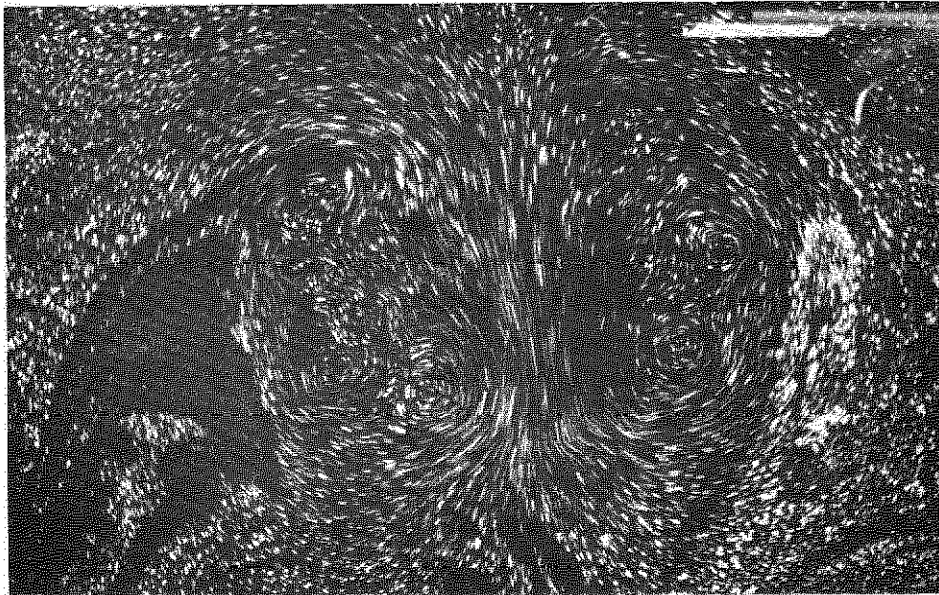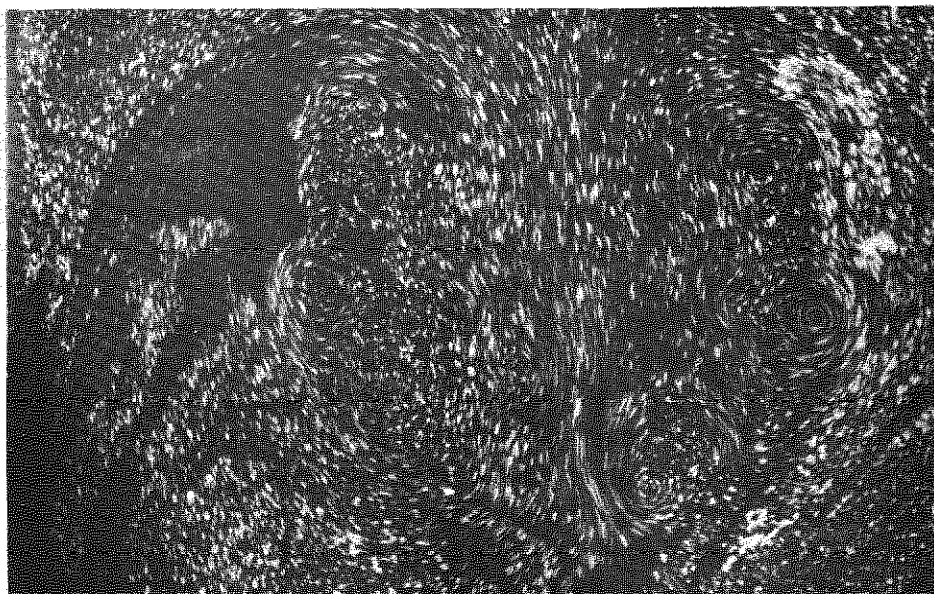
t(s)
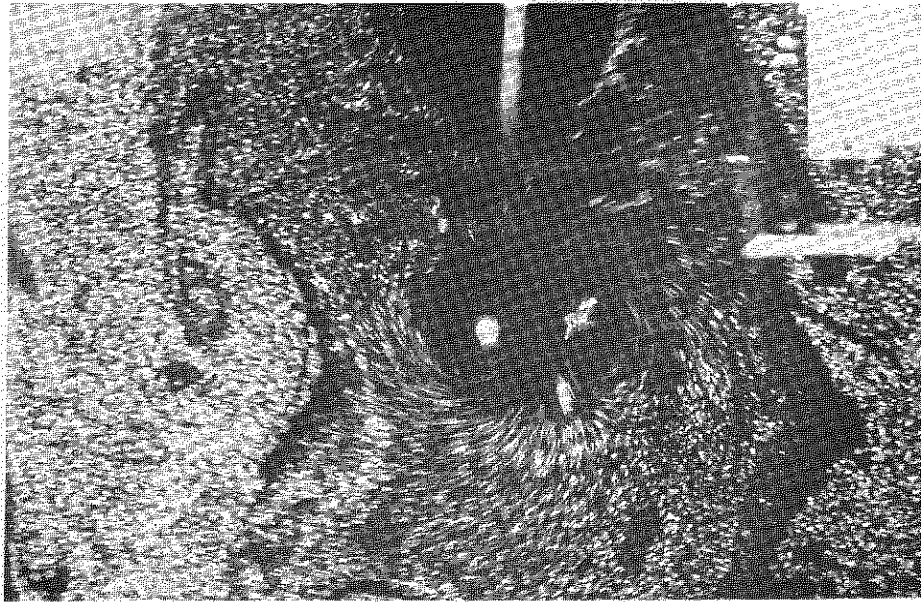
3
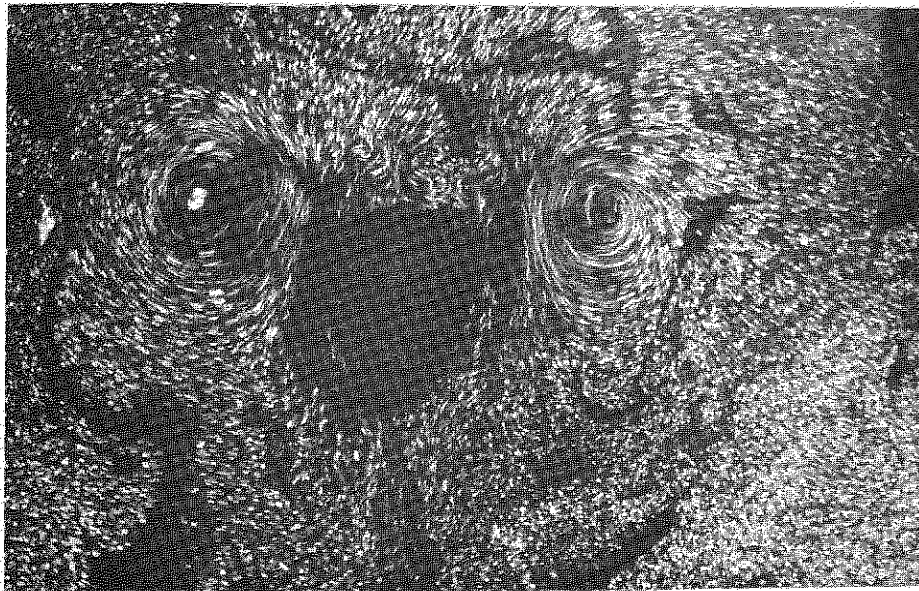
10·5
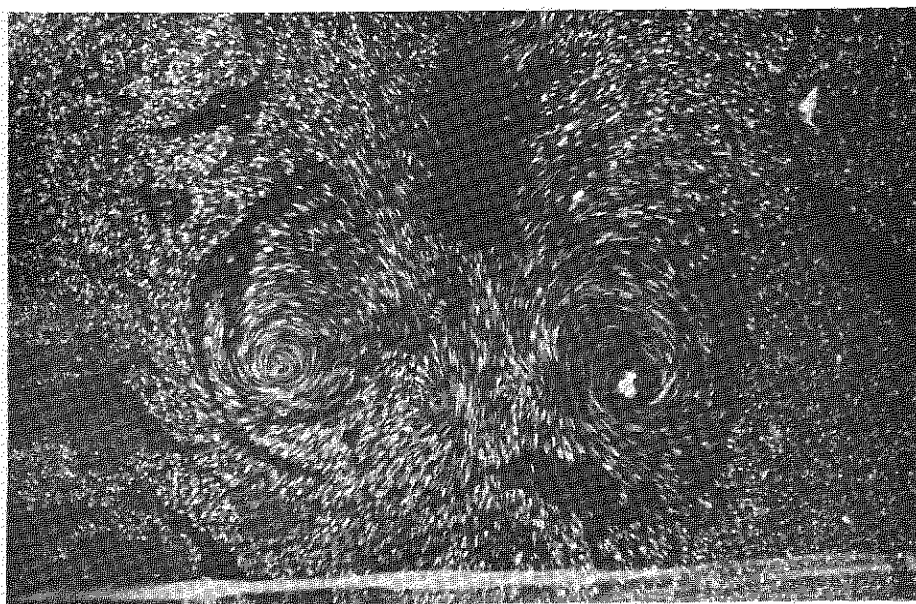
15

Wake patterns: delta wing, $\alpha = 12°$, U = 2·4 ft/s.
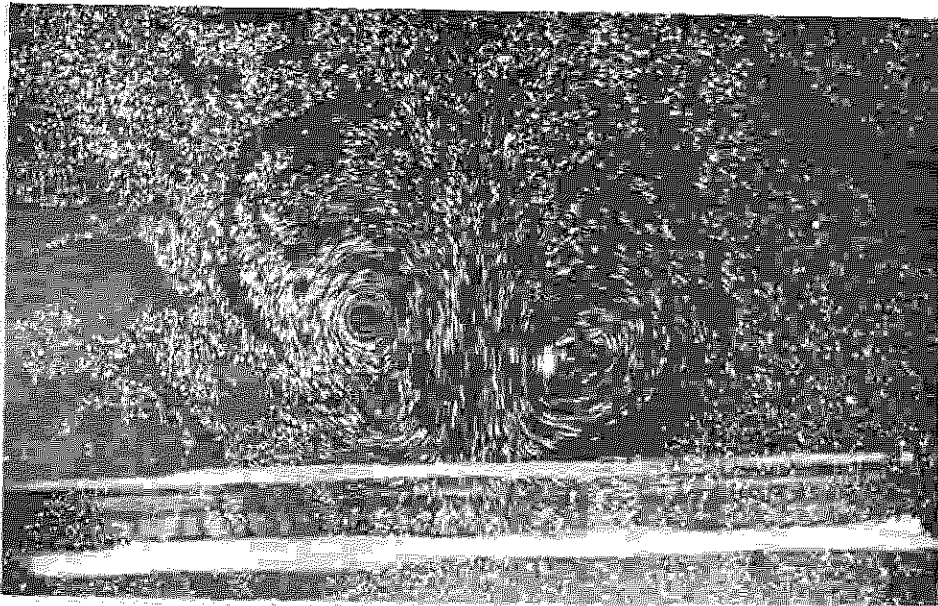
t(s)

19·5
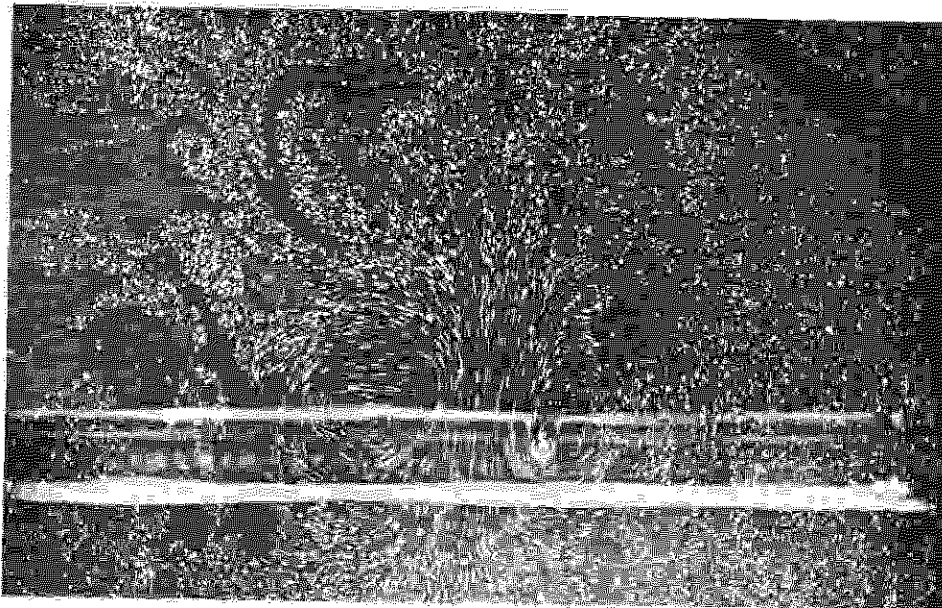
25
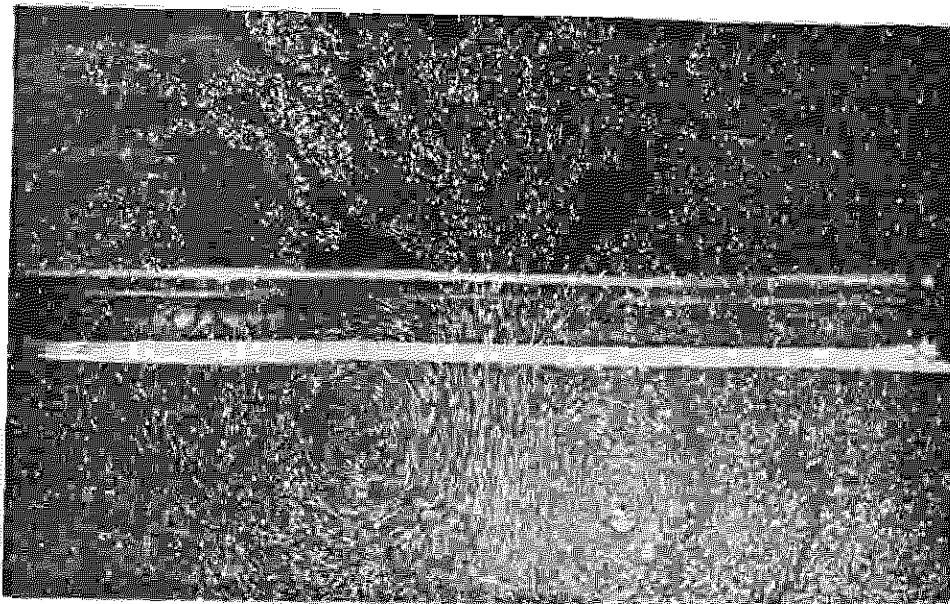
35·5

$\frac{1}{4}$ s exp·

FIG. 14 (contd.)

33215
FIG 15
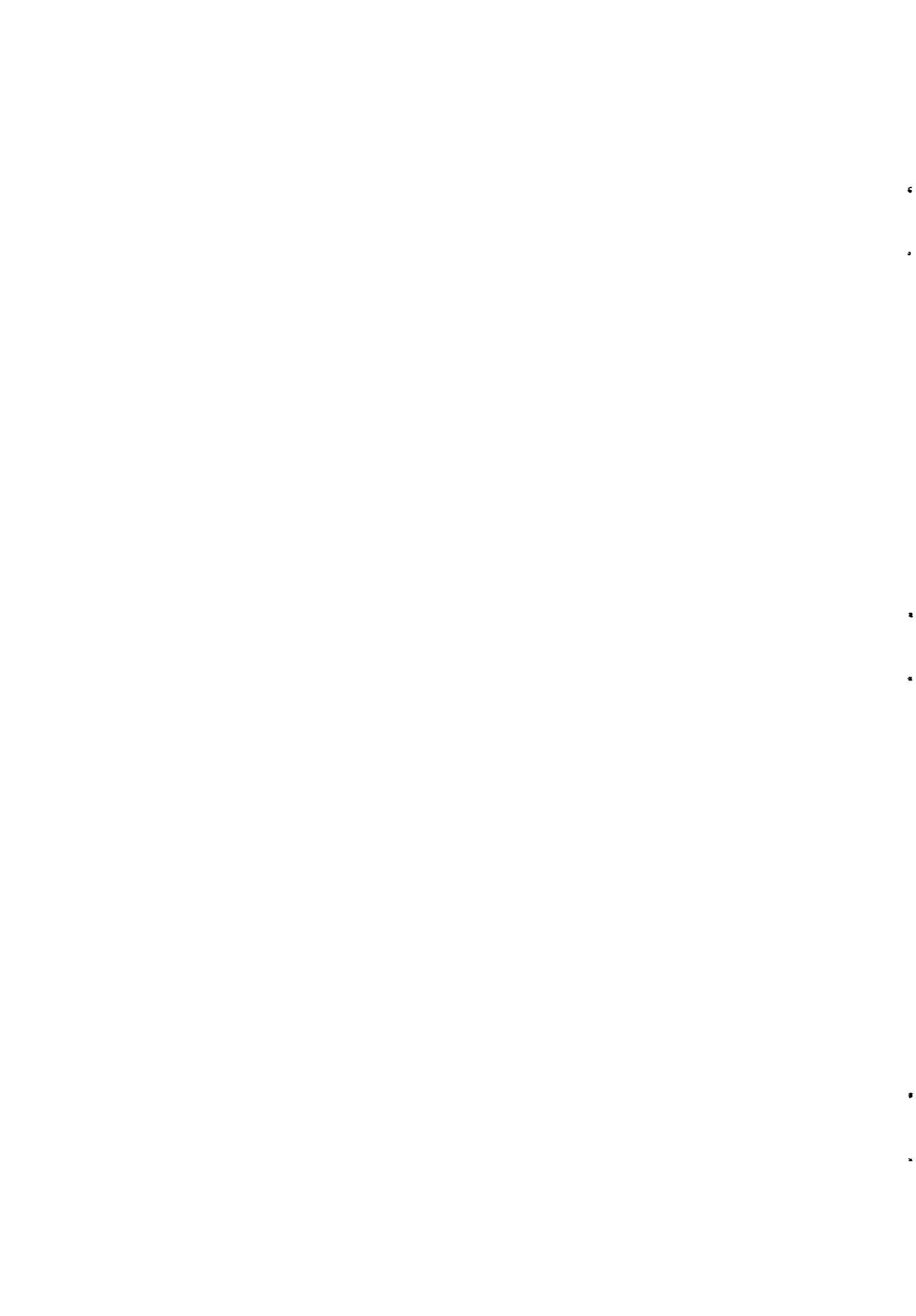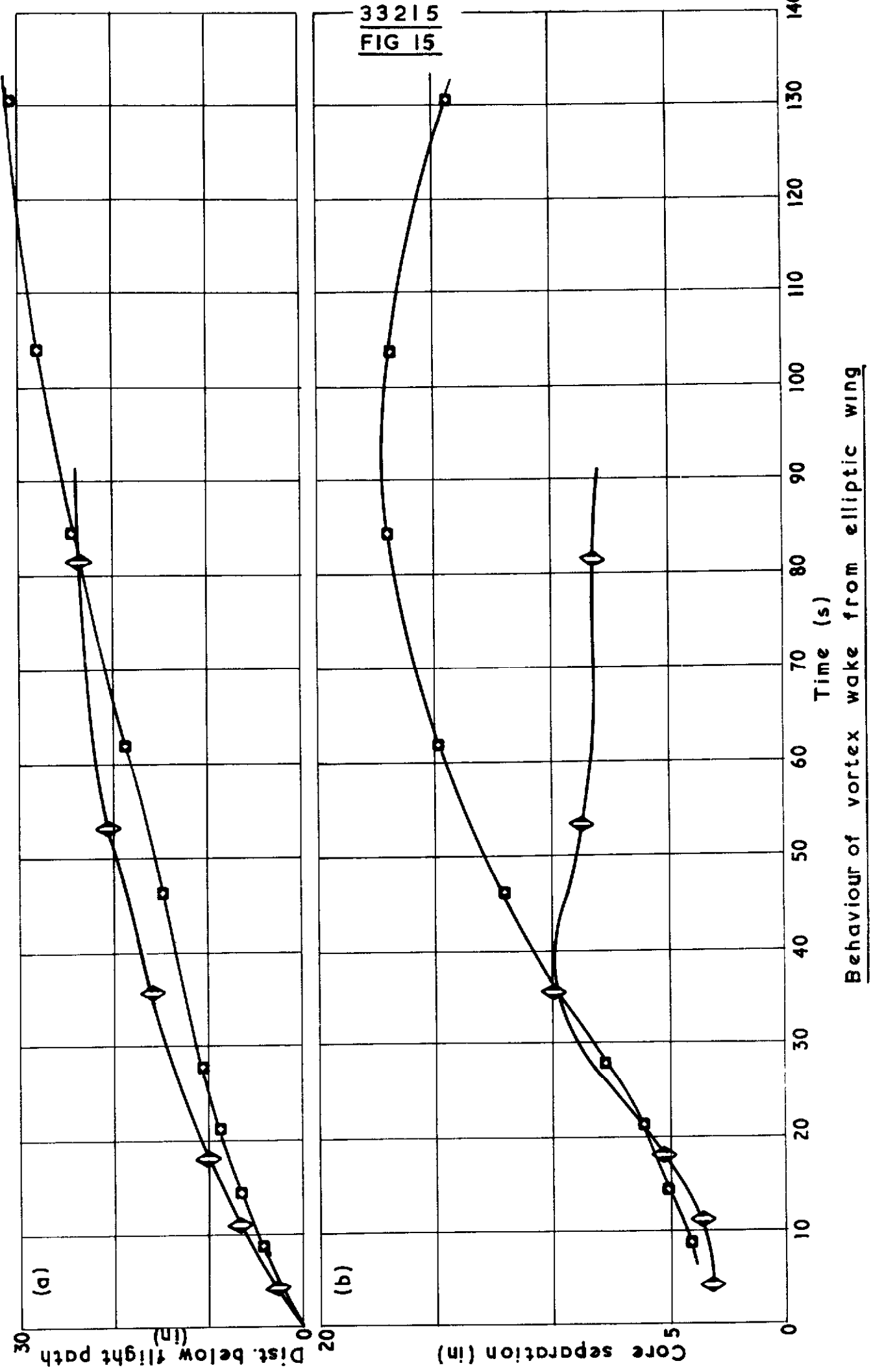
Behaviour of vortex wake from elliptic wing
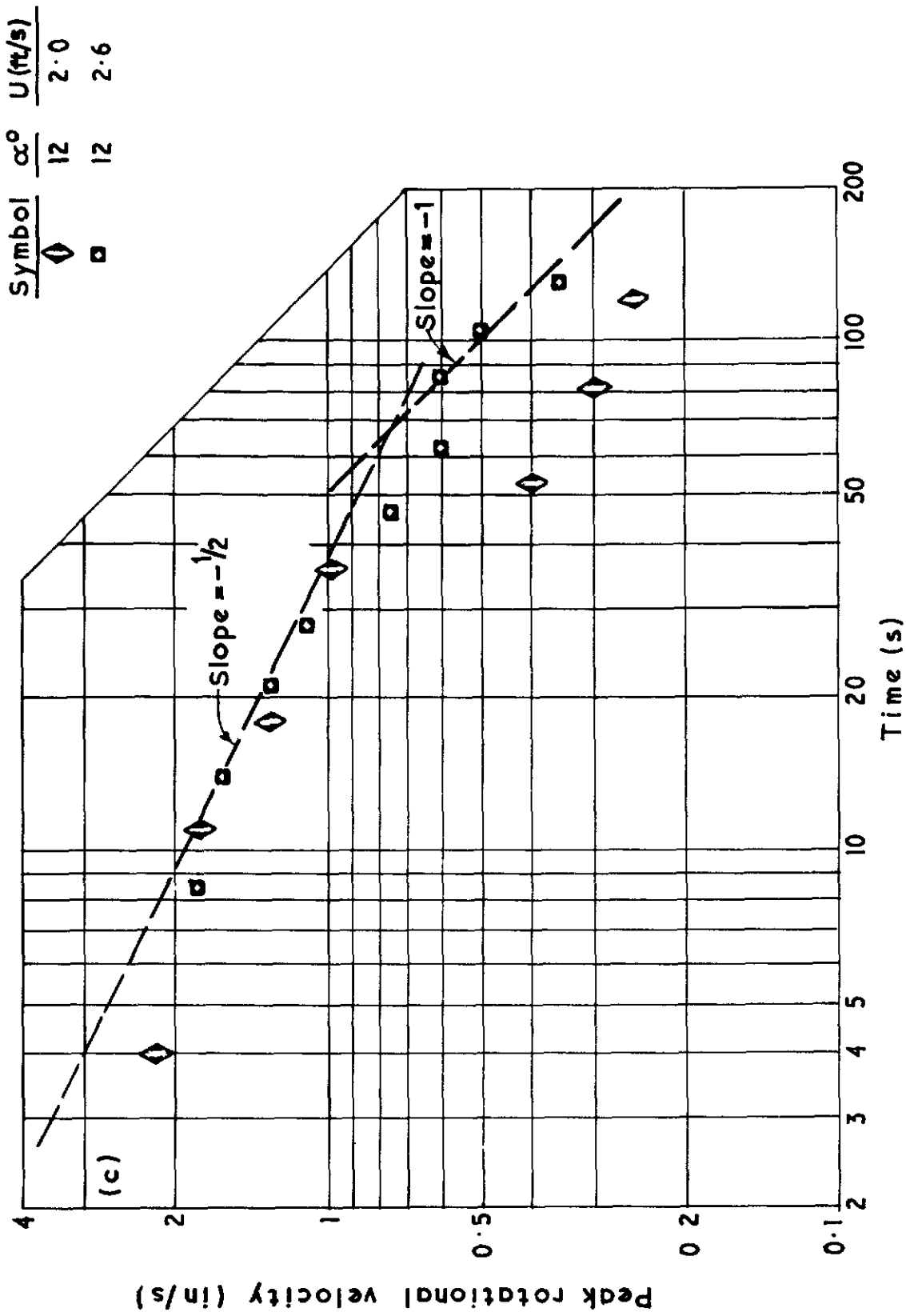
FIG 15 (contd.).
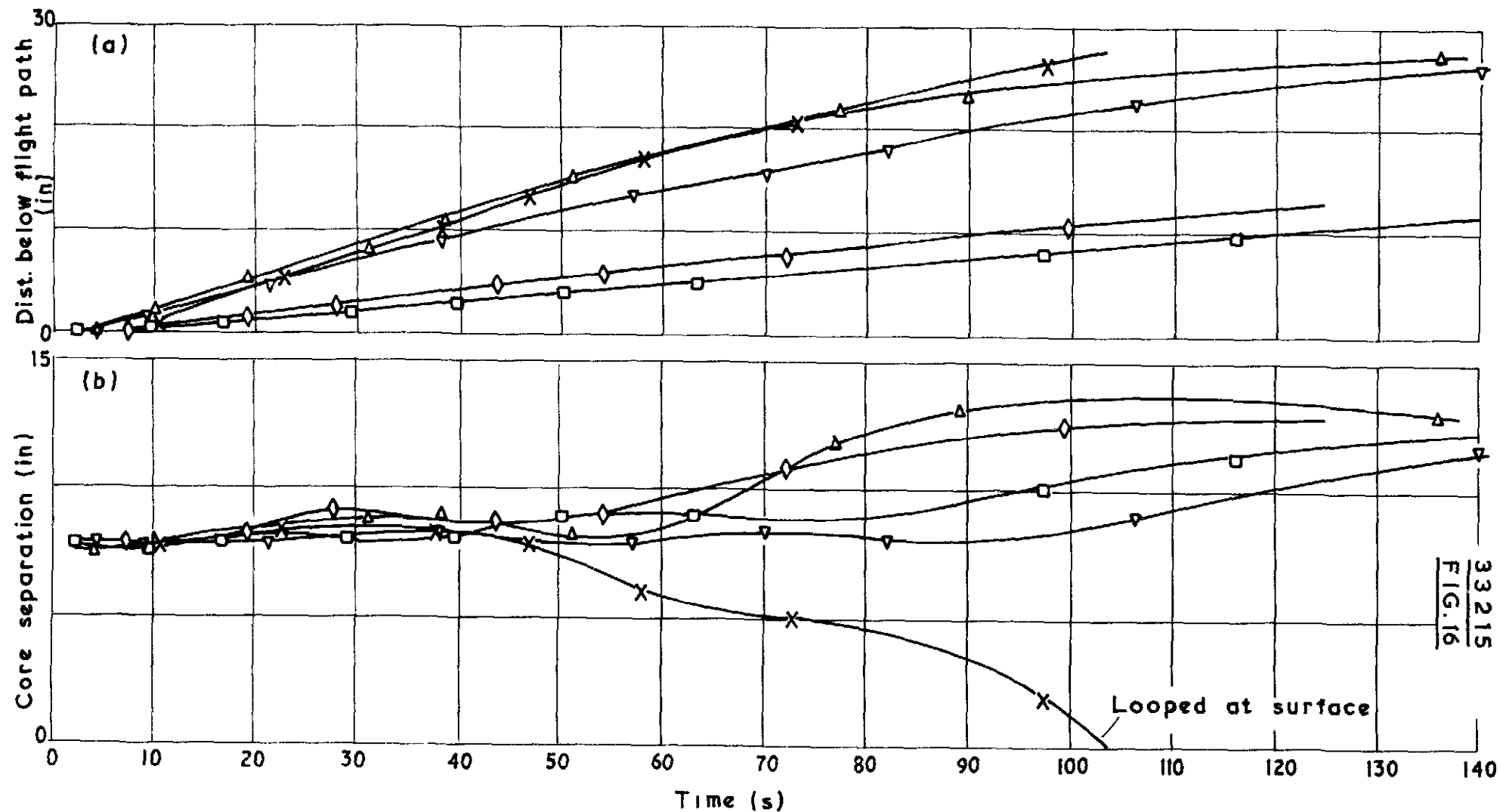
Behaviour of vortex wake from rectangular wing

Symbol	α°	U (ft/s)
□	5	2·3
◇	5	3·0
▷	10	2·2
◁	10	3·1
X	10	2·6

Peak rotational velocity (in/s)

Time (s)

FIG. 16 (contd)

(a)

Dist. below flight path (in)

(b)

Core separation (in)

Time (s)

Behaviour of vortex wake from swept wing

(c)
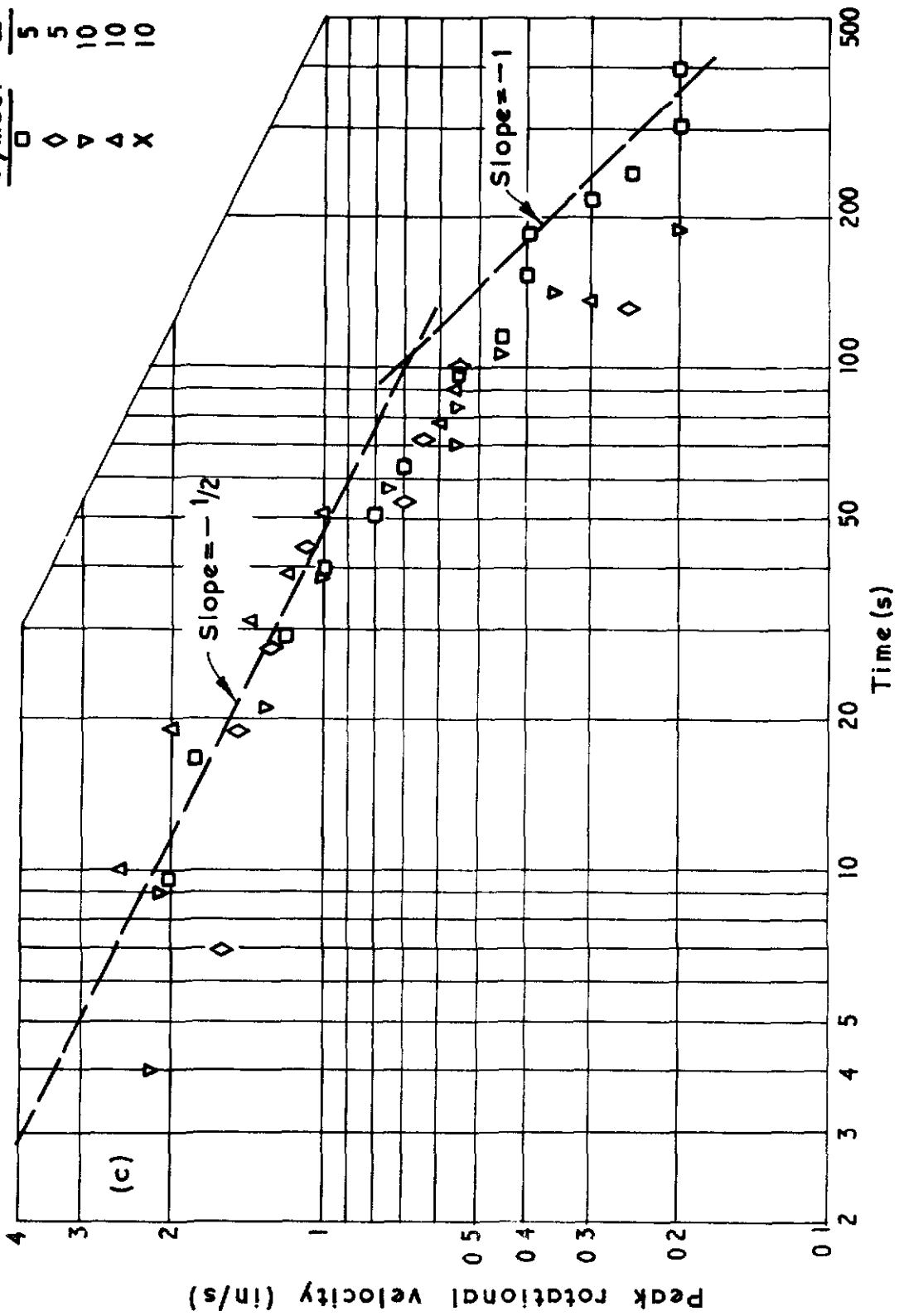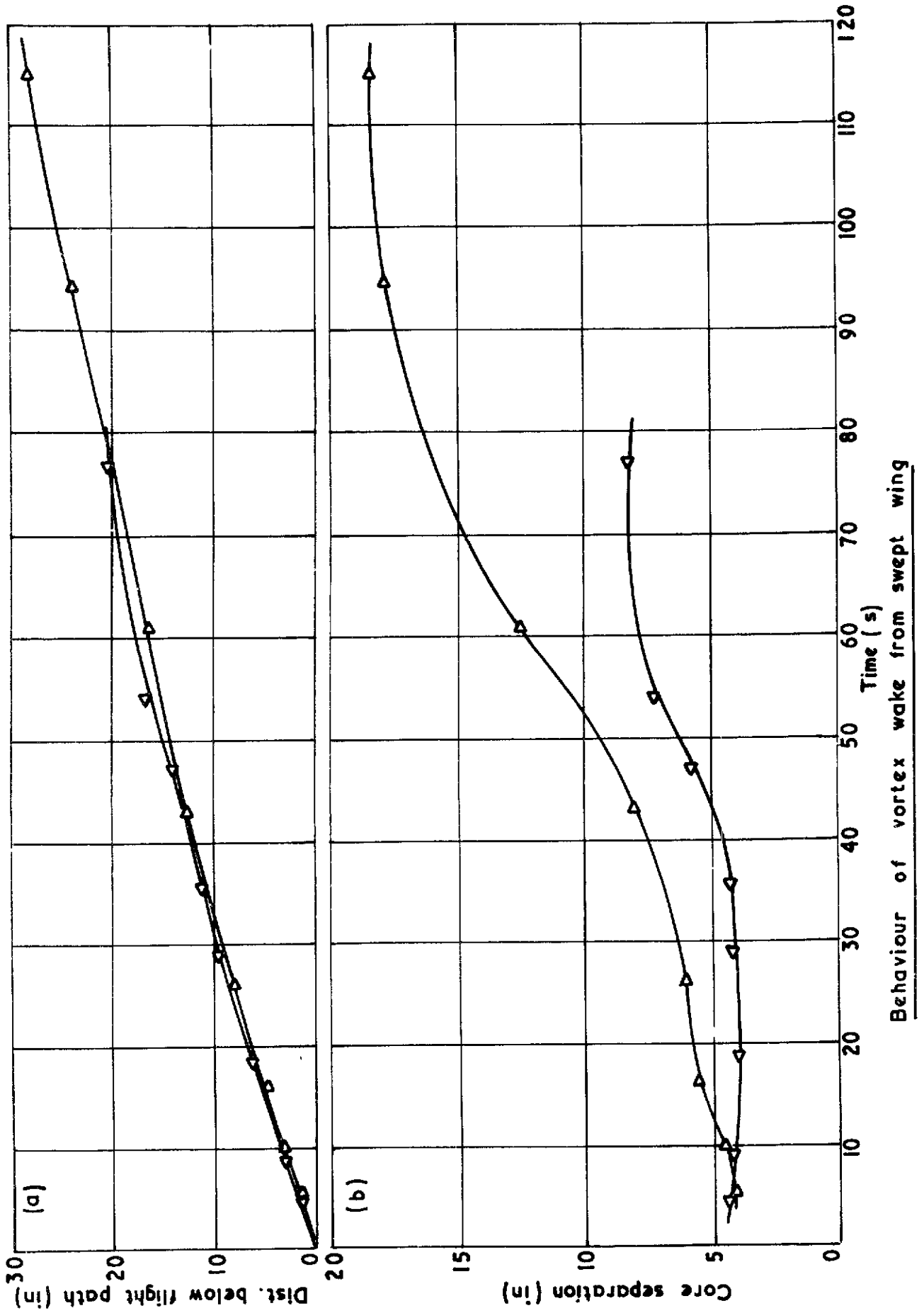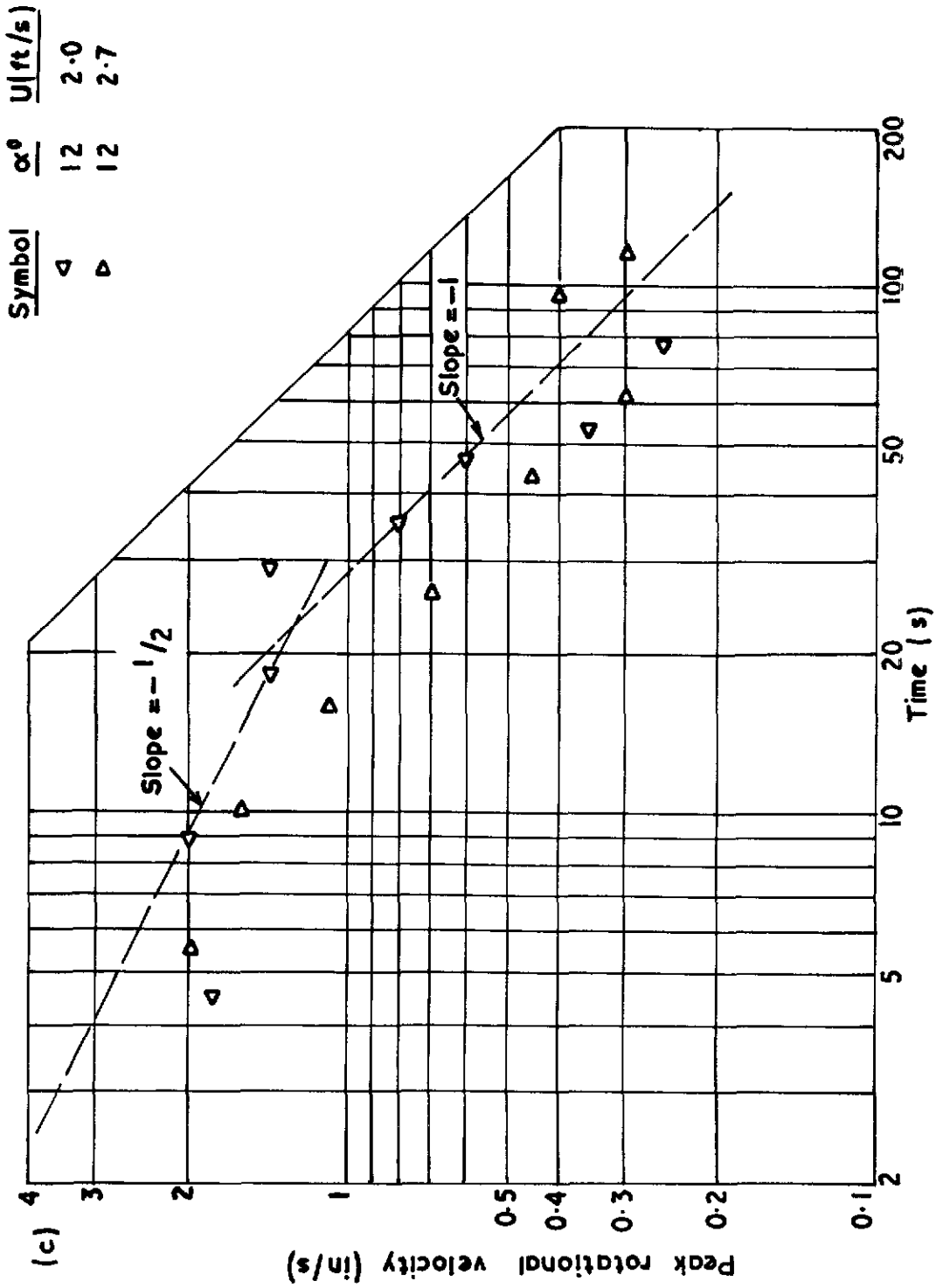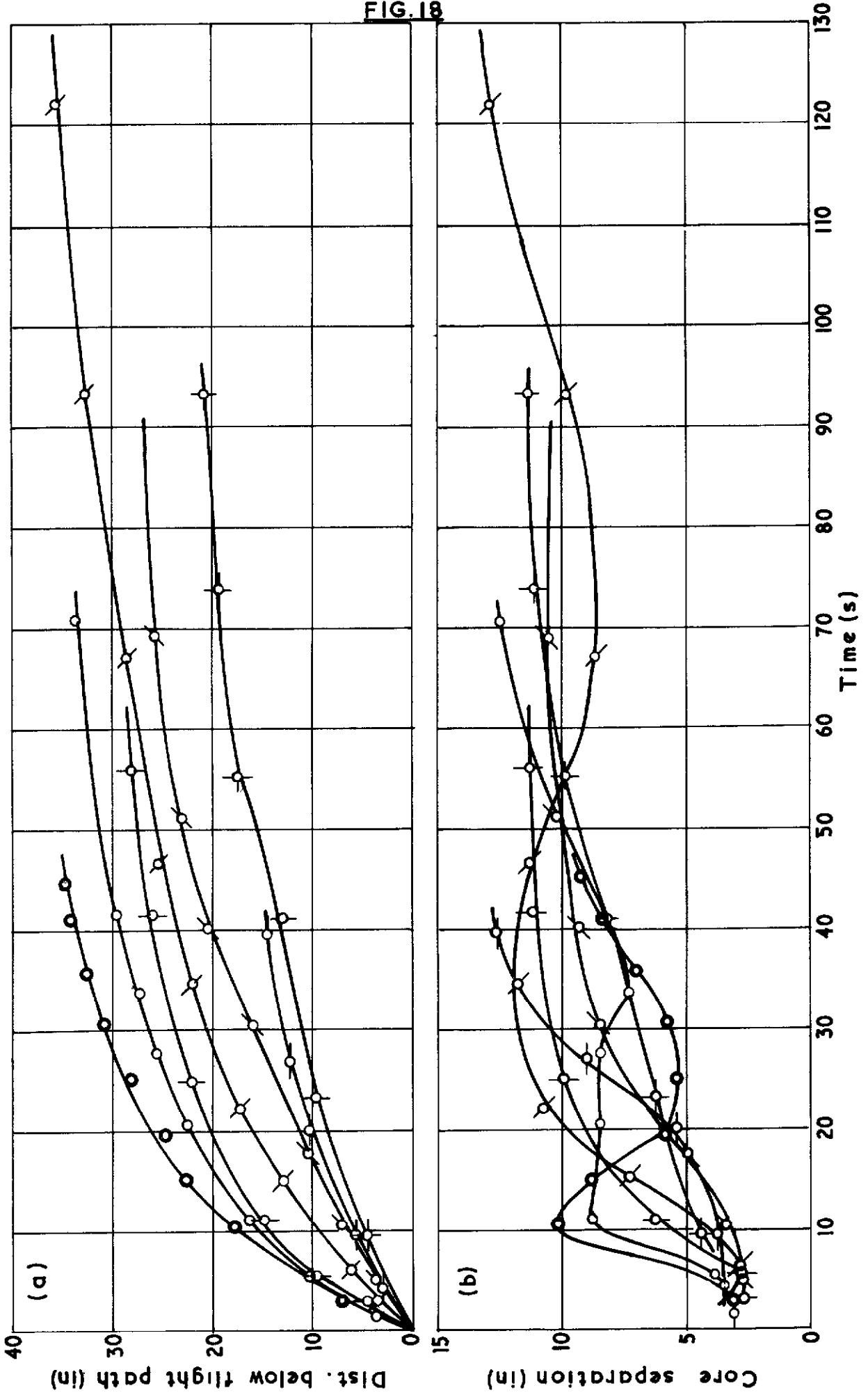
Behaviour of vortex wake from delta wing

33215
FIG.18. (contd.)
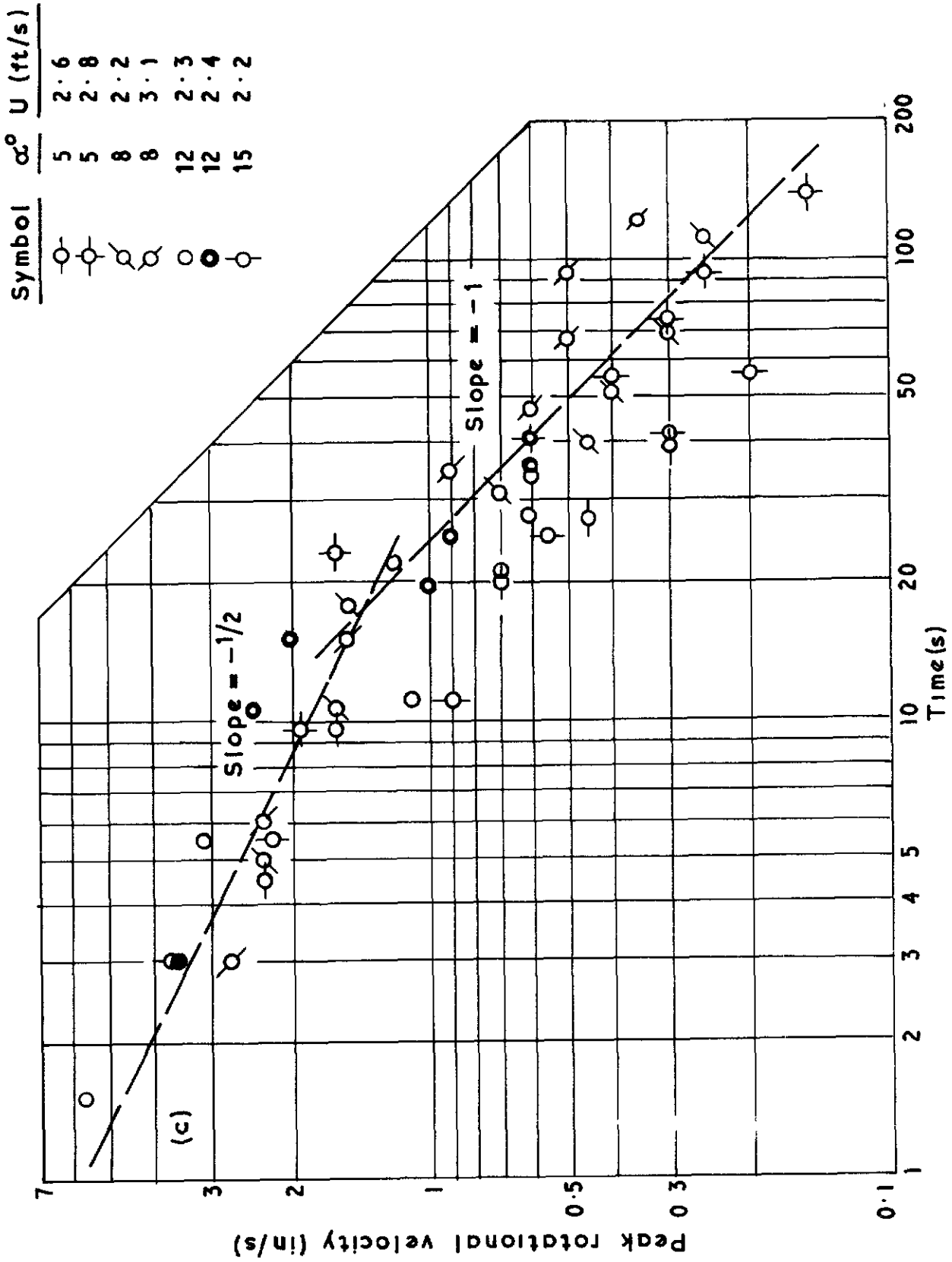
FIG 18. (contd)
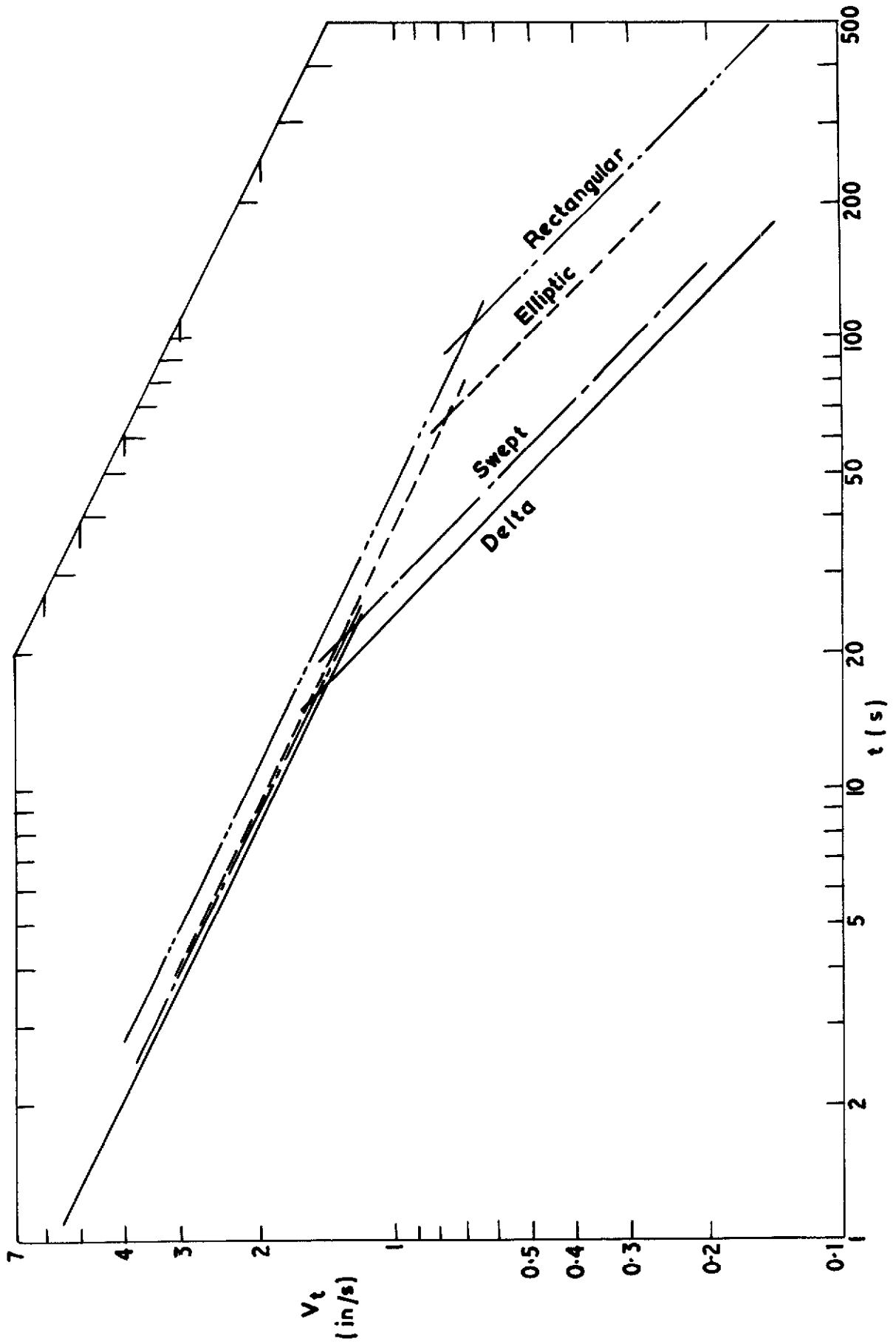
General comparison of velocity decay for different wings

Upper bounds from HP115 tests (see Ref.14)

Slope = –1

$a = 4 \times 10^{-4}$

$a = 2 \times 10^{-4}$

Slope = –½

$\dfrac{t}{b_o'^2} (\sin^{-2})$

Non-dimensionalised velocity decay

$\dfrac{v_t \, b_o'^2}{a_1 \propto US}$ (in ft^{-1})

(a_1 estimated from wing geometry)

33 215
FIG. 2

Non-dimensionalised velocity decay.
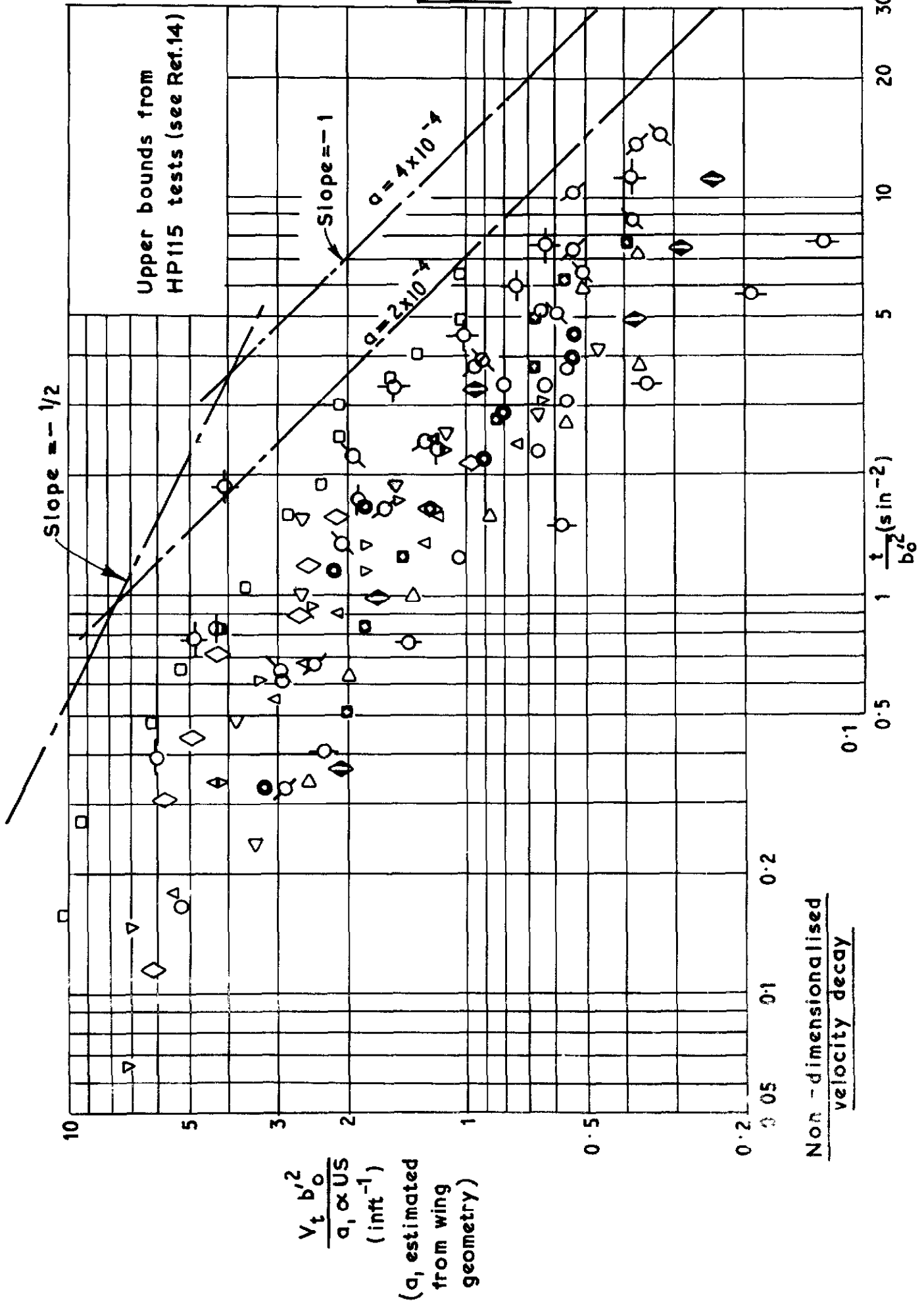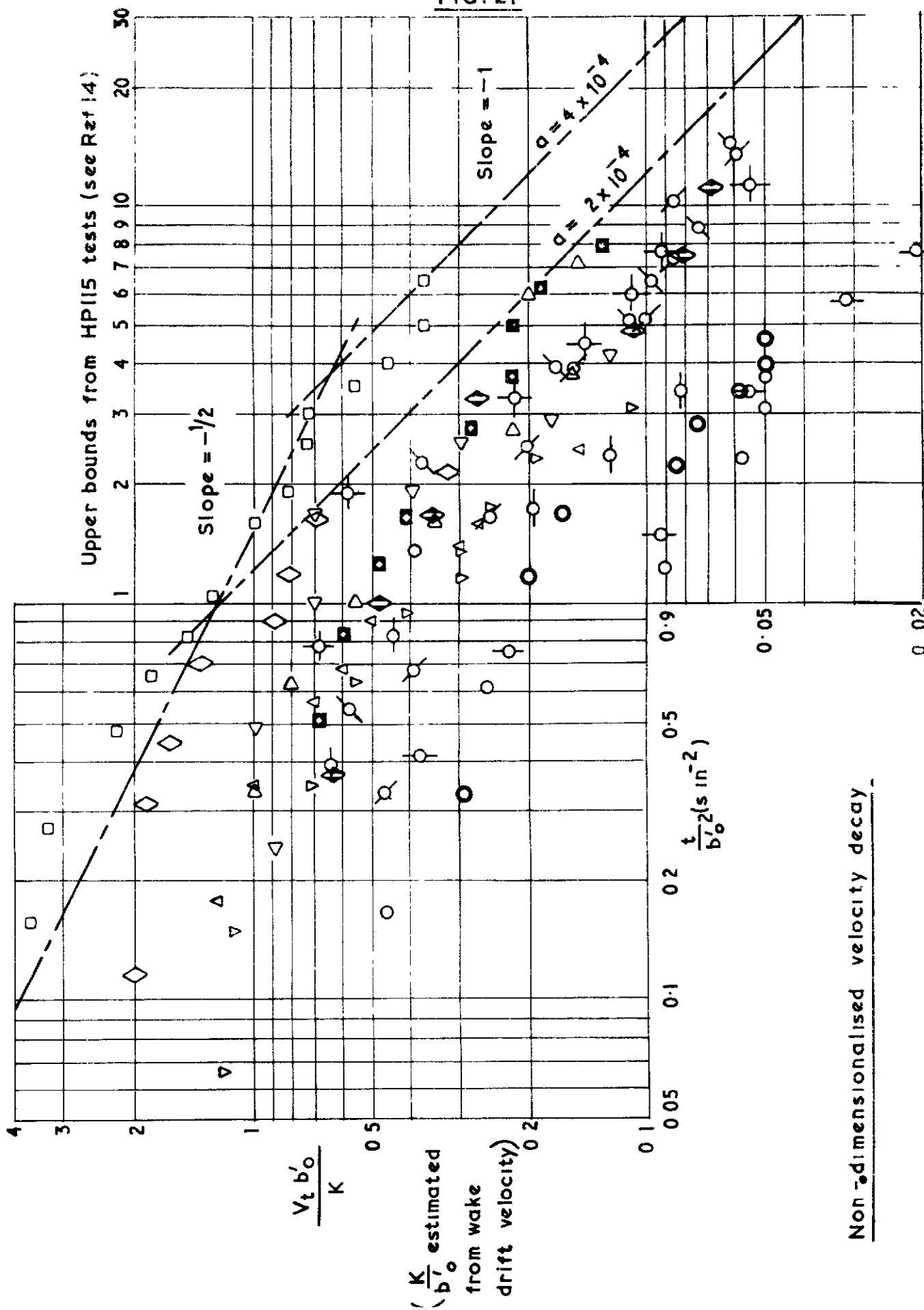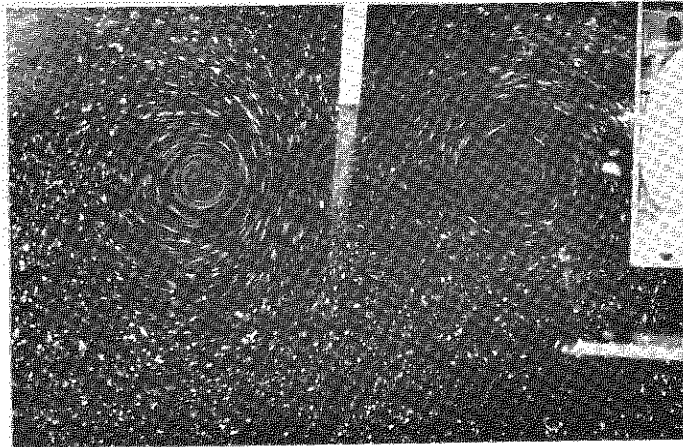
Rectangular wing: $\alpha = 5°$, U = 2·3 ft/s,
t = 16·5 s

Delta
wing

Rectangular
wing

Core centres

Delta wing: $\alpha = 5°$, U = 2·6 ft/s,
t = 4·5 s

Comparison of velocity distributions

(a)

(b)

FIG A.

K_1 ○

○K_2

(a)

Stagnation point

K_1○

K_2 ○

(b)
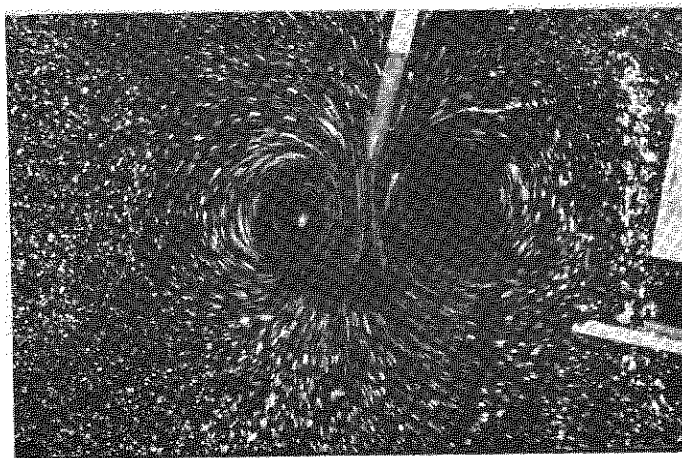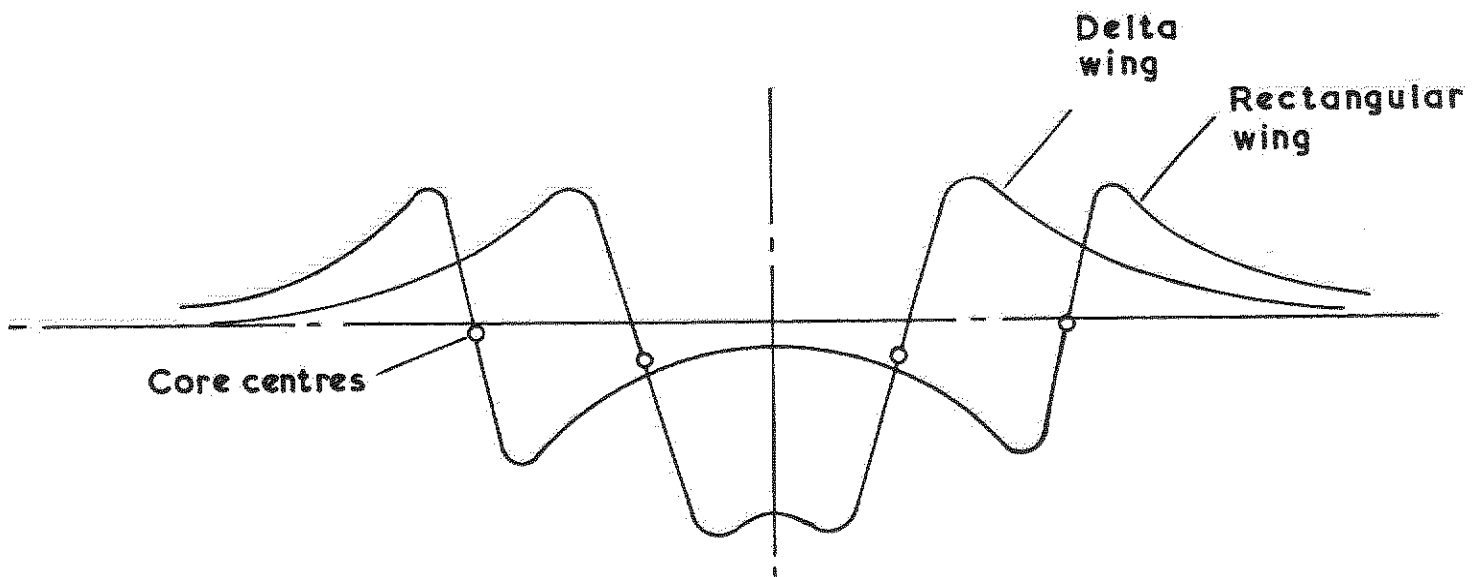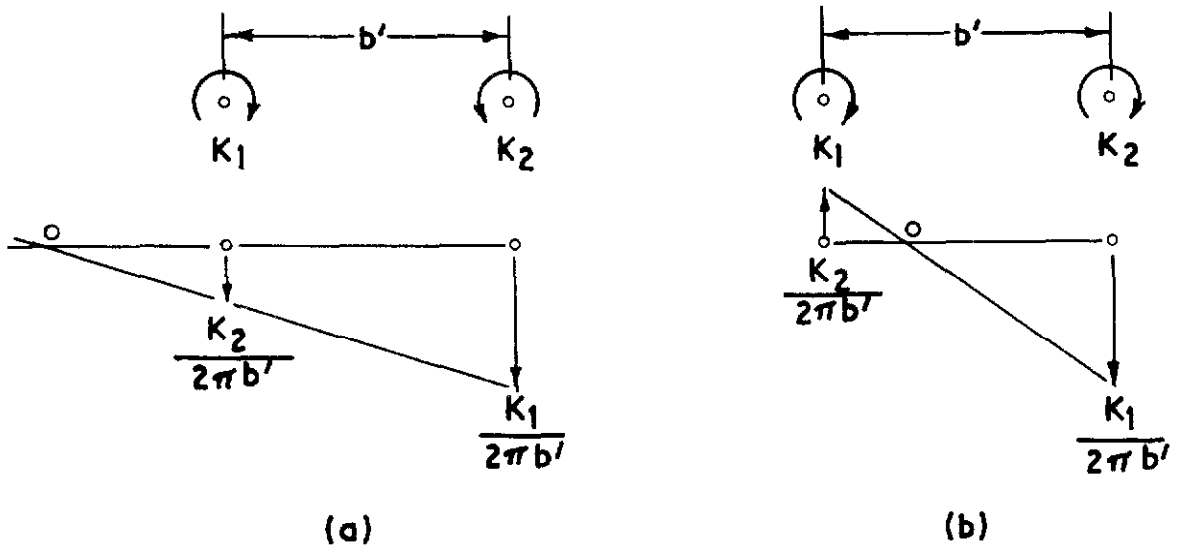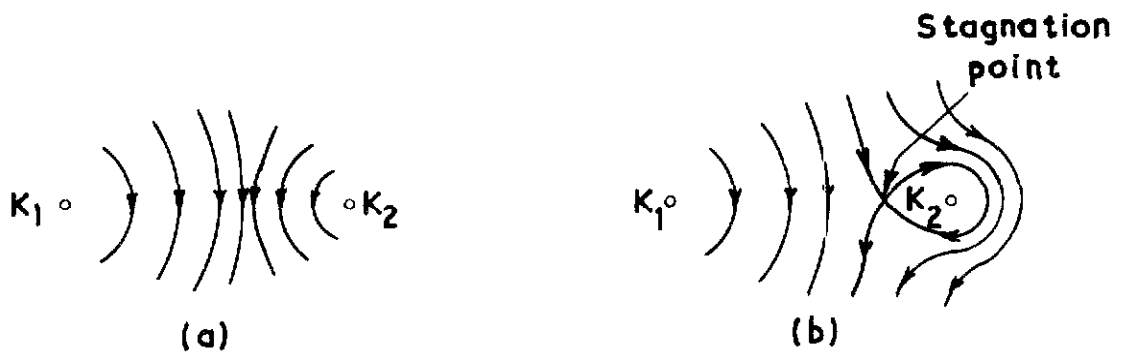
FIG. B.
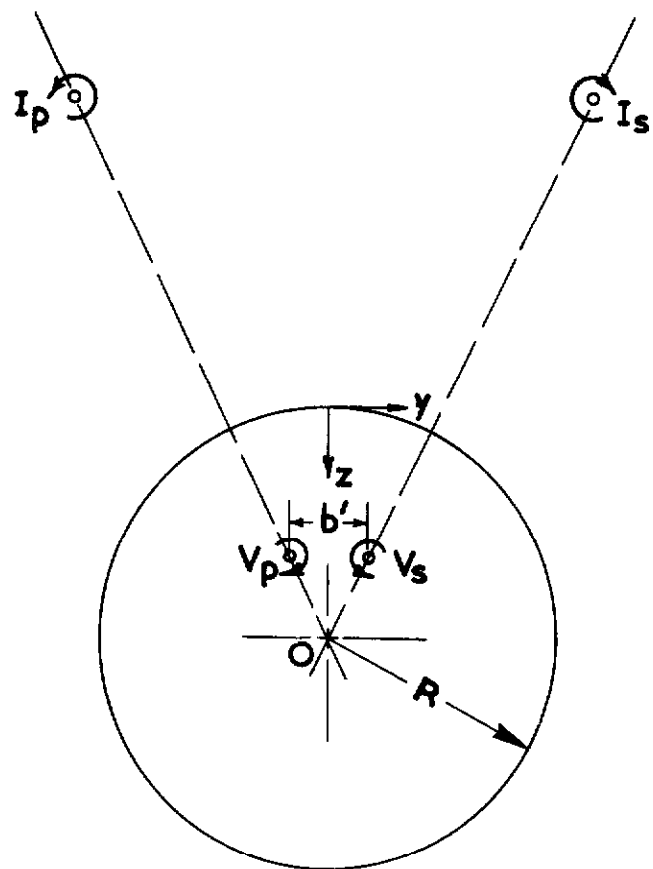
FIG. C.
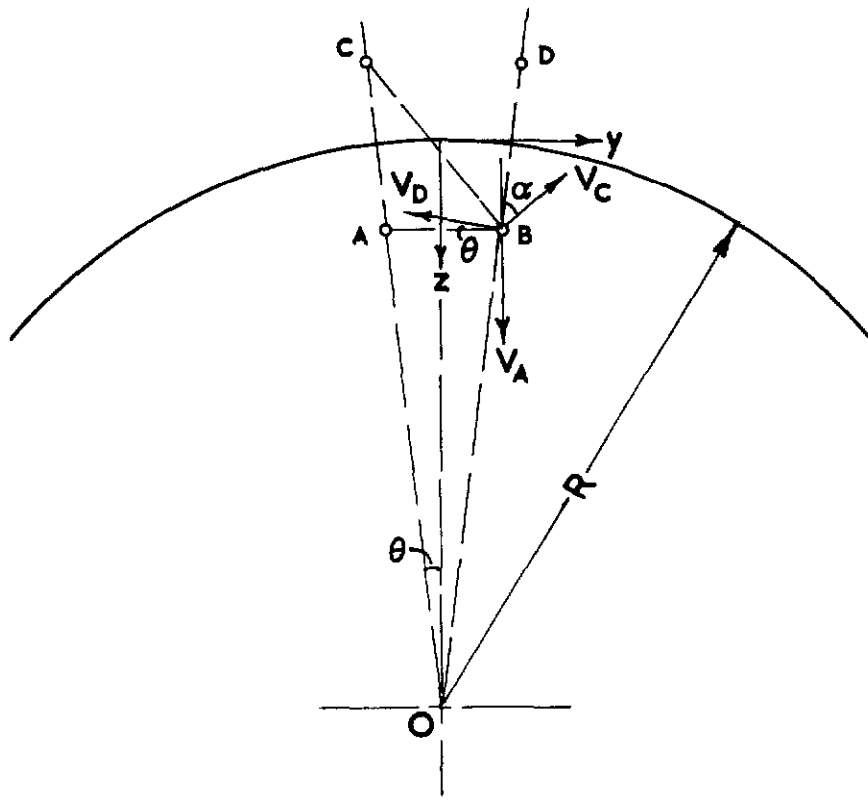
FIG.D.
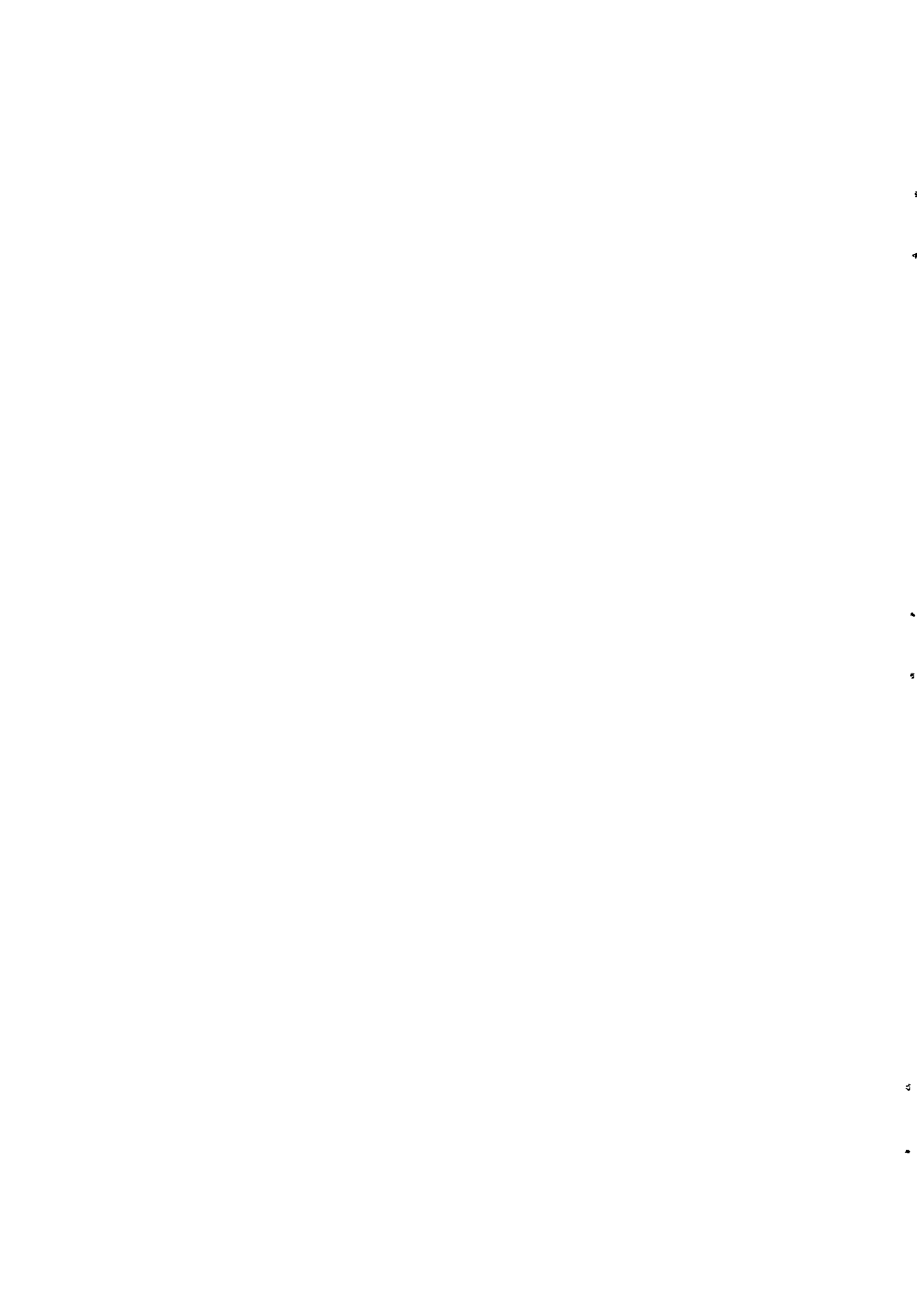
ARC CP No.1238
June, 1971
Oon, E. H.

DECAY OF TRAILING VORTICES

Model wings of various planforms were plunged vertically into a water tank and the vortex patterns on the surface were studied.

For each wing the wake drift rate was found to increase with incidence and to decrease with increasing core separation. The wake started off with discrete vortex cores which grew independently, maintained their initial separation, and had peak velocities which decayed as t time$^{-\frac{1}{2}}$. The edges of the cores ultimately came very close together, and thereafter separation distance between the core centres increased with time, and the peak velocities tended to decay at time^{-1}.

SBN 11 470796 0